
This EarthArXiv preprint is a non-peer reviewed version of the manuscript submitted to AMS Artificial Intelligence for the Earth Systems (AIES). Copyright may be transferred without further notice.

Sub-seasonal Prediction of Central European Summer Heatwaves with Linear and Random Forest Machine Learning Models

Elizabeth Weirich Benet,^a Maria Pyrina,^a Bernat Jiménez Esteve,^a Ernest Fraenkel,^b Judah
Cohen,^{c,d} and Daniela I.V. Domeisen^{a,e}

^a *Institute for Atmospheric and Climate Science, ETH Zürich, Zürich, Switzerland*

^b *Department of Biological Engineering, MIT, Cambridge, USA*

^c *Atmospheric and Environmental Research (AER), Lexington, USA*

^d *Department of Civil and Environmental Engineering, MIT, Cambridge, USA*

^e *Institute of Earth Surface Dynamics, Université de Lausanne, Lausanne, Switzerland*

Corresponding author: Elizabeth Weirich Benet (weiriche@ethz.ch) and Daniela I.V. Domeisen
(daniela.domeisen@env.ethz.ch)

16 **ABSTRACT:** Heatwaves are extreme near-surface temperature events that can have substantial
17 impacts on ecosystems and society. Early Warning Systems help to reduce these impacts. However,
18 state-of-the-art prediction systems can often not make accurate forecasts of heatwaves more than
19 two weeks in advance, which are required for advance warnings. We therefore investigate the
20 potential of statistical and machine learning methods to understand and predict central European
21 summer heatwaves on time scales of several weeks. As a first step, we identify the most important
22 atmospheric and surface predictors based on previous studies and supported by a correlation
23 analysis: 2-m air temperature, 500-hPa geopotential, precipitation, and soil moisture in central
24 Europe, as well as Mediterranean and North Atlantic sea surface temperatures, and the North
25 Atlantic jet stream. Based on these predictors, we apply machine learning methods to forecast
26 summer temperature anomalies and the probability of heatwaves for 1–6 weeks lead time at weekly
27 resolution. For each of these two target variables, we use both a linear and a Random Forest model.
28 The performance of these models decays with lead time, as expected, but outperforms persistence
29 and climatology at all lead times. For lead times longer than two weeks, our machine learning
30 models beat the European Centre for Medium-Range Weather prediction system. We thus show
31 that machine learning can help extend the forecasting lead time of summer temperature anomalies
32 and heatwaves.

33 SIGNIFICANCE STATEMENT: Heatwaves (prolonged extremely warm temperatures) cause
34 thousands of fatalities worldwide each year. These damaging events are becoming even more
35 severe with climate change. This study aims to improve advance predictions of summer heatwaves
36 in central Europe by using statistical and machine learning methods. Machine learning models are
37 shown to outperform conventional physics-based models for forecasting heatwaves more than two
38 weeks in advance. These early warnings can be used to activate effective and timely response plans
39 targeting vulnerable communities and regions, thereby reducing the damage caused by heatwaves.

40 1. Introduction

41 A heatwave is an extended period of extremely hot weather relative to the expected local con-
42 ditions at that time of the year. These high temperatures can cause substantial damage to human
43 health, agriculture, infrastructure, and biodiversity (Perkins 2015; Barriopedro et al. 2011). How-
44 ever, although heatwaves are among the most dangerous natural hazards, their corresponding death
45 and destruction tolls are not always immediately obvious (Wallemacq et al. 2018; Basu 2002; Lowe
46 et al. 2011), making heatwaves *silent killers* (Loughnan 2014). Between 1998 and 2017, globally
47 more than 166'000 people died due to heatwaves – the 2003 European heatwave alone caused
48 70'000 deaths (Wallemacq et al. 2018). In addition, the probability of other natural disasters,
49 such as wildfires, is higher during heatwaves (e.g., the Australian wildfires 2020 ignited amid a
50 record-breaking heatwave (Deb et al. 2020)). Furthermore, the variability of global temperature is
51 increasing with climate change. Combined with global warming, this trend results in more extreme
52 hot weather (Perkins 2015; Barriopedro et al. 2011). As a consequence of climate change, heat-
53 waves are increasing in intensity, duration, and frequency (Ford et al. 2018; Perkins and Alexander
54 2013; Perkins-Kirkpatrick and Lewis 2020; Seneviratne et al. 2014).

55 Early warning systems (EWS) are one of the most effective climate adaptation measures (WMO
56 2021), because they enable effective and timely response plans that target vulnerable populations
57 and regions. For instance, EWSs help to determine when crops will need more irrigation or when
58 local hospitals must prepare for an additional number of patients (Bassil and Cole 2010). However,
59 the time needed to prepare for heatwaves is often beyond the time scales of medium-range weather
60 forecasts (up to two weeks) that are currently available (de Perez et al. 2018). While long-term
61 averages on seasonal time scales show some predictability, a gap of forecast skill between two weeks

62 and seasonal scales remains (White et al. 2017; Robertson et al. 2015). Alternative approaches
63 must therefore be explored to extend the lead time of skillful forecasts to sub-seasonal time scales
64 (two weeks to two months).

65 A variety of machine learning (ML) and deep learning (DL) models have been used for extreme
66 weather forecasting (Reichstein et al. 2019; Cho et al. 2020; Khan et al. 2019; Kretschmer et al.
67 2017; Lehmann et al. 2020; Liu et al. 2016; Racah et al. 2016; Chattopadhyay et al. 2020). Other
68 studies have focused on ML-based summer temperature and heatwave forecasting (Kämäräinen
69 et al. 2019; Pyrina et al. 2021; Vijverberg et al. 2020; Sobhani et al. 2018). However, these studies
70 target either seasonal instead of sub-seasonal scales (Kämäräinen et al. 2019; Pyrina et al. 2021),
71 North America instead of central Europe (CE) (Vijverberg et al. 2020; Sobhani et al. 2018), or focus
72 on identifying physical drivers of heatwaves and not on a comparison of the model performance
73 to dynamical prediction models (van Straaten et al. 2022). Moreover, summer heatwaves have
74 stronger impacts due to the absolute temperatures they reach, leading to higher mortality rates than
75 in winter (US EPA 2016). This makes summer heatwaves more harmful than winter heatwaves,
76 which are usually associated with milder conditions.

77 In this study, we investigate central European sub-seasonal forecasting of summer heatwaves
78 using statistical and ML methods. We aim at answering the following research questions:

79 (i) Which predictors are the most relevant for sub-seasonal forecasts of summer temperature
80 anomalies in CE?

81 (ii) Can the sub-seasonal forecasting accuracy of summer temperature anomalies and heatwaves
82 in CE be improved by using ML methods based on the predictors identified in (i)?

83 In order to answer these two questions, we first select a set of atmospheric and surface predictors
84 which, based on previous studies, are thought to have the largest impact on heatwave prediction
85 (Perkins and Alexander 2013; Li et al. 2020; Perkins 2015; Zschenderlein et al. 2020; Suarez-
86 Gutierrez et al. 2020; Oliveira et al. 2020; Bladé et al. 2011; Dong et al. 2013; Ossó et al. 2020;
87 Mecking et al. 2019; Duchez et al. 2016; Black et al. 2004; Fischer et al. 2007; Kolstad et al. 2017;
88 Seneviratne et al. 2010). We consider both remote drivers, which are linked to CE temperatures
89 via teleconnections, and local drivers (see Sec 2). Additionally, we conduct a linear correlation
90 analysis between each potential predictor and 2-m air temperature. We then use these predictors
91 as the input for ML models to forecast summer temperature anomalies and the probability of

92 heatwaves at lead times from one to six weeks. For each of the two forecast problems we use both a
93 linear model and a random forest (RF) model. The methods are presented in Section 3, the results
94 and limitations of our study are discussed in Sections 4 and 5, respectively, and we conclude in
95 Section 6.

96 We show that ML models can help extend the forecasting lead time of summer temperature
97 anomalies and heatwaves when compared to the European Centre for Medium-Range Weather
98 Forecasts (ECMWF) prediction system. These improved forecasts can be used to enhance EWS.

99 **2. Physics of heatwaves**

100 Summer heatwaves differ from winter heatwaves, as they are driven by different mechanisms:
101 while winter European heatwaves are mainly driven by warm air advection from the equator, sum-
102 mer European heatwaves are based on persistent high-pressure systems (blocking highs) (Perkins
103 and Alexander 2013; Li et al. 2020; Perkins 2015; Zschenderlein et al. 2020). We therefore expect
104 forecasting models that are trained separately for summer and winter to perform better and focus
105 exclusively on drivers of summer heatwaves.

106 By reviewing the physical mechanisms behind central European summer heatwaves, we identify
107 a set of relevant predictors. First, the local geopotential associated with blocking anticyclones and
108 upper level ridges can drive summer heatwaves on short time scales (up to a couple of weeks)
109 (Suarez-Gutierrez et al. 2020; Kautz et al. 2022). Hereby, the geopotential at the 500-hPa pressure
110 level is typically used to avoid capturing the bidirectional influence between surface temperature
111 and surface pressure (i.e., the high temperature leading to low pressure near the ground) (Suarez-
112 Gutierrez et al. 2020). Second, leading modes of large-scale atmospheric variability relevant for
113 summer European climate are found to be linked to the latitude and speed of the North Atlantic
114 (NA) jet stream (Oliveira et al. 2020). The occurrence and persistence of weather regimes can be
115 used to characterise the location and intensity of the NA storm track, thus acting as key predictors
116 for near-surface temperature extremes over Europe (Bladé et al. 2011; Dong et al. 2013). In
117 particular, the Summer East Atlantic (SEA) pattern (i.e., the second dominant mode of summer
118 low-frequency variability in the Euro-Atlantic region) can significantly influence temperatures and
119 precipitation over Europe during summer months Wulff et al. (2017).

120 Third, cold sea surface temperature (SST) anomalies in the NA are found to be present prior to
121 the onset of the most extreme European heat waves since 1980 (Duchez et al. 2016). For instance,
122 anomalously cold SSTs in the NA were key to the development of the 2015 European heatwave
123 (Mecking et al. 2019). Moreover, northwestern Mediterranean (NWMED) SSTs are linked to
124 temperatures over the European continent due to their proximity and large heat capacity, acting
125 as a heat buffer for land temperatures (e.g., the 2003 European heatwave was connected to warm
126 Mediterranean SSTs) (Black et al. 2004).

127 Furthermore, precipitation is associated with low pressure systems (cyclones). During a cyclone,
128 clouds reduce the amount of solar radiation reaching the surface, which results in less sensible heat
129 flux and a lower surface air temperature. Finally, precipitation directly influences soil moisture,
130 which is a further driver of summer heatwaves (Fischer et al. 2007). A drying pattern (low soil
131 moisture) and warming reinforce each other due to a positive feedback effect (Kolstad et al. 2017):
132 If soil is moist, the incoming solar radiation is used more towards latent heat flux to the atmosphere,
133 whereas, if soil is dry, it emits more sensible heat. For this reason, drier soil will heat up faster than
134 moist soil. This will, in turn, result in less soil moisture and thus, in even more dryness, closing the
135 positive feedback loop (Seneviratne et al. 2010); if the preceding winter and spring have been dry,
136 extremely high summertime temperatures are more likely to occur over Europe (Perkins 2015).

137 **3. Methods**

138 *a. Heatwave index definitions*

139 We define weekly heatwaves via a binary index: one for a heatwave week and zero, otherwise.
140 While there is no universal definition for heatwaves and a range of different indices are found across
141 the literature, percentile-based definitions are widely used (Perkins 2015; Perkins and Alexander
142 2013; Perkins-Kirkpatrick and Lewis 2020; Spensberger et al. 2020). We use two different heatwave
143 definitions: $+1\sigma$ for high and $+1.5\sigma$ for extremely high temperature anomalies (see Fig 1). The
144 $+1\sigma$ weekly heatwave index is defined as one for the weekly mean temperature anomalies above
145 one standard deviation (σ) (i.e., to the right of the orange line in Figure 1) and zero, otherwise.
146 Analogously, the $+1.5\sigma$ weekly heatwave index is defined as one for the weekly mean temperature
147 anomalies above 1.5 standard deviations (i.e., to the right of the red line in Figure 1) and zero,
148 otherwise.

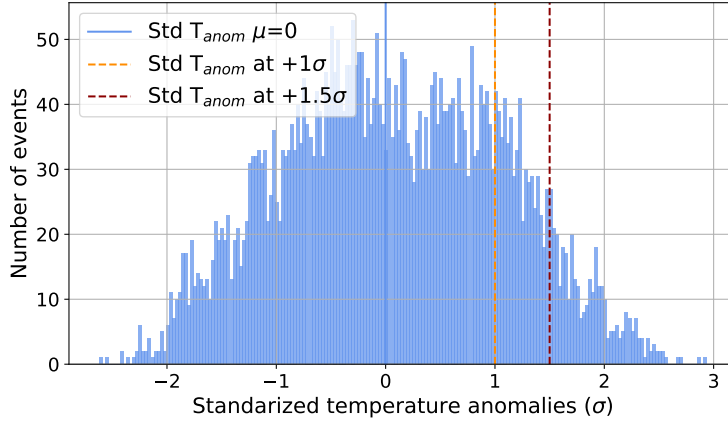


FIG. 1: **Histogram of temperature anomalies for the definition of heatwave indices** The blue bars correspond to the standardized ($\mu = 0$, $\sigma = 1$) temperature anomalies. The data is smoothed by a 7-day running mean (see Sec 3b2). The vertical blue line marks the mean ($\mu = 0$) of the distribution. The stippled orange (red) line marks $+1$ ($+1.5$) standard deviations (σ) from the mean and is used to define heatwaves.

149 *b. Data*

150 1) PREDICTORS

151 We select seven atmospheric and surface predictors that we expect to be related to summer
 152 temperature and heatwaves in CE based on previous studies (see Sec 2) and a correlation analysis
 153 (see Sec 4b1). These predictors are: 2-m air *temperature*, 500-hPa *geopotential*, *precipitation*, *soil*
 154 *moisture*, the *SEA* index, *NWMED SST*, and *cold North Atlantic anomaly (CNA) SST*. This set of
 155 predictors is considered in the extended summer season (MJJAS), during the time period between
 156 1 May 1981 and 30 September 2018. Further technical details about these predictors can be found
 157 in Table 1. Since both local predictors and remote teleconnections are included, location details
 158 are shown in Figure 2 and their latitude-longitude coordinates are provided in Table 2. Moreover,
 159 to assess the robustness of our models, the analysis is repeated on 110 years of ERA20C data
 160 (1900–2009). The results are similar and are not shown here.

161 (i) *Calculation of the SEA index* The changes in speed and location of the NA jet stream are
 162 included in our set of predictors through the *SEA* index. First, the *SEA* pattern is calculated via
 163 principal component analysis (PCA) (Storch and Zwiers 2003), applied on the detrended 500-hPa
 164 geopotential height anomalies over the NA box for the summer season (JJA). The *SEA* index
 165 corresponds to the time dependent coefficients (or PCA amplitudes) of the second PCA pattern

166 (Wulff et al. 2017). Then, the daily *SEA* index is calculated for the extended summer season
 167 (MJJAS) by projecting the *SEA* pattern on the daily values of the 500-hPa geopotential height
 168 anomalies from May to September. After the index is calculated, the obtained time series are
 169 normalised to a mean equal to zero and standard deviation equal to one.

Predictor	Physical magnitude (units)	Source (Space, Time Res.)	Level	Box	Method
Temperature	2-m air temperature ($^{\circ}\text{C}$)	E-OBS (0.25° , daily)	2 m a.g.	CE	avg
Geopotential	geopotential ($\text{m}^2 \text{s}^{-2}$)	ERA-Interim (2.5° , daily)	500 hPa	CE	avg
Precipitation	thickness of rainfall amount (mm)	E-OBS (0.25° , daily)	surface	CE	avg
Soil moisture	volumetric soil water layer ($\text{m}^3 \text{m}^{-3}$)	ERA5-Land (2.5° , daily)	0–28 cm u.g.	CE	avg
SEA index	geopotential ($\text{m}^2 \text{s}^{-2}$)	ERA-Interim (2.5° , daily)	500 hPa	NA	PCA
NWMED SST	sea surface temperature ($^{\circ}\text{C}$)	HadISST (1° , monthly)	sea level	NWMED	avg
CNAA SST	sea surface temperature ($^{\circ}\text{C}$)	HadISST (1° , monthly)	sea level	CNAA	avg

TABLE 1: **Properties of the predictors** For each predictor, the name of the corresponding variable (physical magnitude) as labeled in the dataset (source) is presented. We also indicate the temporal and spatial resolution at which each variable was downloaded, the extracted vertical level, the selected spatial location, and the method used to convert the two-dimensional latitude-longitude field into a one-dimensional time series. The soil moisture (0–28 cm u.g.) is calculated as the average over the first two layers (layer one: 0–7 cm u.g. and layer two: 7–28 cm u.g.). The monthly SST predictors are interpolated to daily time resolution. Notation: a.g.: above ground and u.g.: underground.

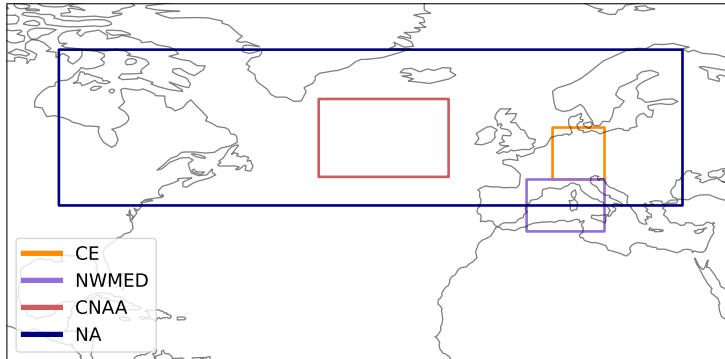


FIG. 2: **Location of latitude-longitude boxes** Used to define the location of the predictors shown in Table 1. The latitude-longitude coordinates of the boxes are shown in Table 2.

170 2) DATA PREPROCESSING PIPELINE

171 (1) First, we select latitude-longitude boxes for each physical magnitude and take either the
 172 average over the corresponding box or perform a PCA (see Tab 1). By removing the spatial

Box	Latitude	Longitude
Central Europe (CE)	45°N–55°N	5°E–15°E
North Atlantic (NA)	40°N–70°N	90°W–30°E
Northwestern Mediterranean (NWMED)	35°N–45°N	0°–15°E
Cold North Atlantic anomaly (CNAА) (Duchez et al. 2016)	45°N–60°N	15°W–40°W

TABLE 2: **Coordinates of latitude-longitude boxes** The boxes correspond to the location of the predictors of Table 1 as seen in Figure 2.

173 dimension, we obtain one-dimensional time series. (2) Second, the maximum overlapping time
174 period for the selected predictors is chosen: 1 May 1981 to 30 September 2018 (38 summers).
175 (3) We then detrend each time series by subtracting the linear trend. Detrending the data removes
176 linear long-term trends. (4) Next, we compute the daily climatology (x_{clim}), which is defined as the
177 mean over the full time period for a particular day of the year. We smooth the daily climatology
178 by a centred 31-day rolling mean window. (5) We then compute the anomalies with respect to
179 climatology as: $x_{\text{anom}} = x - x_{\text{clim}}$. This way, also periodic changes due to seasonality are removed.
180 (6) Afterwards, to reduce the noise caused by natural variability, which might lead to overfitted
181 models, the data is smoothed out via a 7-day centred rolling mean. (7) Then, we standarize the
182 predictors: $x_{\text{std anom}} = \frac{x_{\text{anom}}}{x_{\text{std}}}$, where $x_{\text{std anom}}$ are the standarized anomalies and x_{std} is the standard
183 deviation of the distribution of each predictor. (8) Furthermore, for each of the six prediction lead
184 times (1–6 weeks), the predictors are given to the ML models at four different time lags before
185 initialization time. For example, for a forecast at two weeks lead time (meaning that we are using
186 a model initialized at a lag of two weeks to forecast *temperature* at lag zero), the *precipitation* (p)
187 is provided at lags of two to five weeks (i.e., $p_{\text{lag}2}$, $p_{\text{lag}3}$, $p_{\text{lag}4}$, and $p_{\text{lag}5}$). (9) Finally, since we
188 want to investigate the predictability of summer temperature, only the extended summer months
189 (MJJAS) are selected.

190 *c. Data balance*

191 Forecasting of the two weekly summer heatwave indices defined in Section 3a ($+1\sigma$ and $+1.5\sigma$)
192 results in an imbalanced classification problem. Using these two indices, we obtain imbalanced
193 training sets (e.g., for the $+1.5\sigma$ index, only 7.41 % of the samples belong to the positive class). A
194 classifier trained on these imbalanced data will learn to always forecast the negative class, leading to
195 a trivial model. Balancing the data before the training and optimizing the probability threshold (see

196 Sec 3f) are two potential solutions to this problem. For this study, we find that the combination of
 197 both methods yields the best results. Therefore, an additional data-balancing step must be added by
 198 the end of the preprocessing pipeline (see Sec 3b2). Two different approaches have been explored
 199 and are compared in this study: (1) We **undersample** the dataset by selecting a random subset of
 200 examples from the negative class, to obtain a 50/50 ratio between positive and negative classes
 201 (Lemaitre et al. 2017). Yet, the size of the training set is considerably reduced by doing so (e.g.,
 202 from 4'437 training samples to 658 for the $+1.5\sigma$ index). (2) Alternatively, we **oversample** the
 203 dataset by repeating randomly selected examples from the positive class until a 50/50 ratio between
 204 positive and negative classes is achieved (Lemaitre et al. 2017). This approach increases the size of
 205 the training set (e.g., from 4'437 points to 8'216 for the $+1.5\sigma$ index), although the number of inde-
 206 pendent samples remains the same. The same information for the $+1\sigma$ index is provided in Table 3.

Weekly heatwave index	$+1\sigma$	$+1.5\sigma$
Percentage of samples in the positive class	20.0%	7.41%
Number of training samples (undersampling)	1'772	658
Number of training samples (oversampling)	7'102	8'216

TABLE 3: **Data balance** Size of the full training set (initially with 4'437 samples) after under-/ and oversampling.

208 *d. Machine Learning models*

209 For our study, we choose models at the two extremes of the bias-variance tradeoff (Mehta et al.
 210 2019). (1) The more simple linear models are prone to have high bias, meaning that the model will
 211 match the training set less closely. These models have a higher potential for under-fitting. Linear
 212 models, however, have low variance, meaning that the predictions of the model do not fluctuate
 213 much with a change of dataset. Overall, these models are focused on the larger trends rather than
 214 on the complicated patterns of the training set. (2) Instead, the more complex RFs are likely to
 215 overfit the data, but also to capture most of the relevant patterns. They tend to have high variance,
 216 but low bias. Here, two models out of each of these two families are used for the regression and
 217 classification forecasts. The multilinear regression (MLR) and the ridge classifier (RC) belong to

218 the *linear model*, and the random forest regressor (RFR) and the random forest classifier (RFC)
219 belong to the *ensemble* modules from *Sklearn*, respectively (Pedregosa et al. 2011).

220 1) LINEAR MODELS

221 Linear regression models forecast the target y as a linear combination of n predictors x_i :

$$\hat{y}(\boldsymbol{\omega}, \boldsymbol{x}) = \omega_0 + \omega_1 x_1 + \dots + \omega_n x_n \quad (1)$$

222 where ω_0 is the intercept and ω_i ($0 < i \leq n$) are the regression coefficients. The coefficients are
223 chosen to minimize the residual sum of squares between the forecast (\hat{y}) and the observed target
224 (y): $\min_{\boldsymbol{\omega}} \|\hat{y} - y\|$. Linear classification models first convert binary targets to $\{-1, 1\}$ and then treat
225 the problem as a regression task. The forecasted class corresponds to the sign of the regressor's
226 forecast. For classification, we use Ridge regularization to control excessively fluctuating functions
227 by adding an additional penalty term in the error function, such that the coefficients do not take
228 extreme values (Mishra 2018). Ridge shrinks the predictor coefficients based on the L2-norm
229 ($\|\boldsymbol{x}\|_2 = \sqrt{\sum_i x_i^2}$). The loss function for minimization then becomes $\|\hat{y} - y\| + \alpha \|\boldsymbol{\omega}\|_2^2$, where the
230 complexity parameter α is a hyper-parameter which controls the amount of shrinkage and is set to
231 1.0.

232 2) RANDOM FORESTS

233 A decision tree makes a recursive partition of the input space into rectangles, by selecting
234 the predictor and the respective cutting point that discriminate best at each node. The resulting
235 leaves (i.e., final nodes) correspond to a specific forecast value (regression) or to a probability
236 of belonging to the positive class (binary classification). However, decision trees have two key
237 disadvantages: (1) Trees usually have high variance due to their greedy split process, which implies
238 that a small change in training data can result in significantly different splits. (2) Since the tree
239 estimate is not smooth, decision trees may not be appropriate when the underlying function is
240 smooth (Khan et al. 2019). A more accurate and robust model can be constructed by creating
241 a random ensemble of uncorrelated decision trees whose averaged prediction is more accurate
242 than that of any individual tree. Random forests use two sources of randomness while training:
243 bagging and feature randomness. (1) Bagging (or bootstrap aggregation) consists in selecting a

244 random subset of the training set with replacement – meaning that individual data points can be
 245 chosen more than once – to train each individual tree. (2) When splitting a node in a classical
 246 decision tree, all features are considered and the one that provides the greatest separation between
 247 observations is selected. In contrast, each individual tree in a RF can pick only from a random
 248 subset of features (Yiu 2019). Finally, the mean or majority-vote forecast of all the regression or
 249 classification trees in the forest is selected as the final result, respectively. RFs are chosen over
 250 other tree-based algorithms, since they are more interpretable (Rudin 2019) than XgBoost and less
 251 prone to overfit than single decision trees.

252 *e. Metrics for the evaluation of forecasting performance*

253 For regression, two different metrics are considered: mean-square error (MSE) and Pearson
 254 correlation. The MSE evaluates how far away the forecasted and the ground truth curves are from
 255 each other and is defined as:

$$\text{MSE} = \frac{1}{T} \sum_{t=1}^T (\hat{y}_t - y_t)^2 \quad (2)$$

256 for y_t the regression dependent variable at time t , \hat{y}_t the predicted value for time t , and T the
 257 number of time steps (sample size). The Pearson correlation measures to what extent the curve
 258 follows the changes and is given by:

$$\text{Corr} = \frac{\sum_{t=1}^T (\hat{y}_t - \bar{\hat{y}})(y_t - \bar{y})}{\sqrt{\sum_{t=1}^T (\hat{y}_t - \bar{\hat{y}})^2} \sqrt{\sum_{t=1}^T (y_t - \bar{y})^2}} \quad (3)$$

259 for $\bar{x} = \frac{1}{T} \sum_{t=1}^T x_t$ the sample mean (i.e., mean over all time steps).

260 For classification, the Receiver Operating Characteristic (ROC) Area Under Curve (AUC) is used
 261 to evaluate the probabilistic forecast. The ROC is the true positive rate (TPR) as a function of
 262 the false positive rate (FPR) (Bradley 1997). The TPR (or Recall) is defined as the proportion of
 263 positive data points that are correctly considered as positive, with respect to all positive data points.
 264 The TPR is given by TP / (FN+TP) for true positives (TPs) and false negatives (FNs). The FPR (or
 265 False Alarm) is defined as the proportion of negative data points that are mistakenly considered as
 266 positive, with respect to all negative data points. The FPR is calculated as FP / (FP+TN) for false

positives (FPs) and true negatives (TNs). Moreover, the performance of the binary classification is assessed via the confusion matrix (see Tab 4) and the geometric mean of the TPR and the FPR (G-Mean), which is defined as $G\text{-Mean} = \sqrt{TPR(1 - FPR)}$ (Brownlee 2020).

We define a *useful* forecast as having a ROC AUC above 0.5 for the probabilistic forecast and a TPR higher than the FPR for the binary classification. For a sensible model, the principal diagonal element values must be high and the off-diagonal element values must be low in the confusion matrix (Bradley 1997).

		Actual value	
		Positive (1)	Negative (0)
Forecasted value	Positive (1)	TP	FP
	Negative (0)	FN	TN

TABLE 4: **Confusion matrix** The positive class corresponds to a heatwave and the negative class to no heatwave.

f. Cross-Validation and hyper-parameter optimization

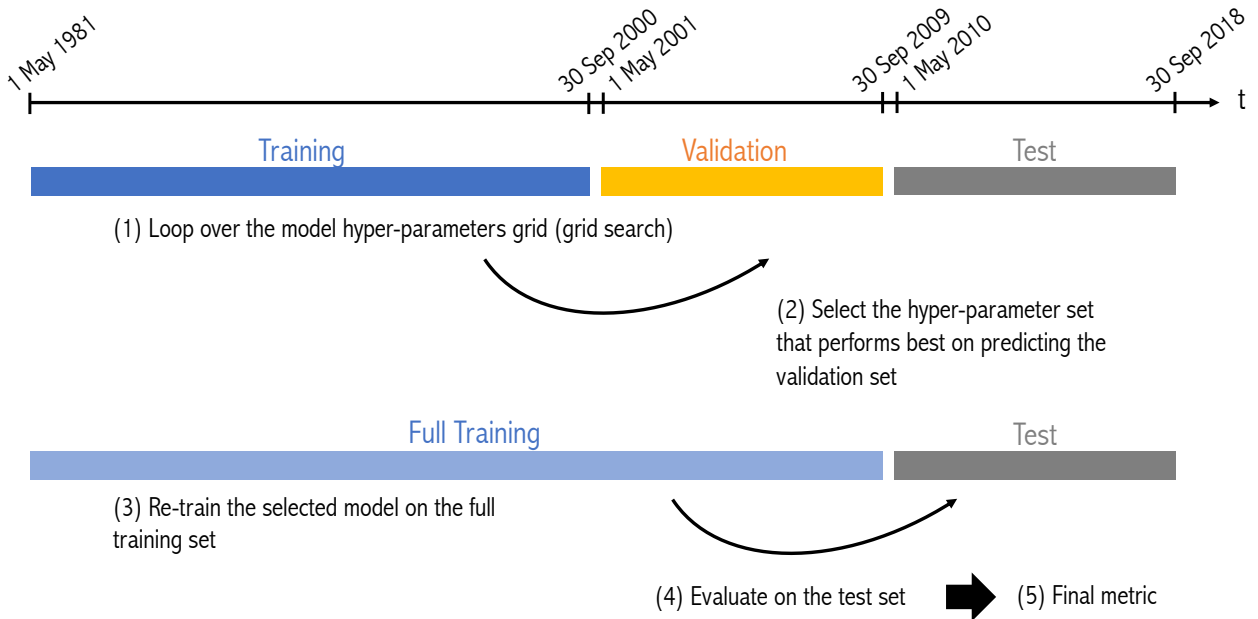


FIG. 3: Schematic of the training-validation-test splits

275 We split the available data into a training period (1 May 1981 – 30 September 2000), a validation
276 period (1 May 2001 – 30 September 2009), and a testing period (1 May 2010 – 30 September
277 2018) (see Fig 3). The validation period is used to optimize the model’s hyper-parameters. After
278 the hyper-parameter optimization, the model is re-trained on the full training period (1 May 1981 –
279 30 September 2009), which is the combination of the validation and the training period. A nested
280 cross-validation (CV) scheme is also implemented (see Fig A1 in the Appendix).

281 For the RFs, we use an exhaustive grid-search hyper-parameter optimization including all
282 possible combinations (750) of the following parameters: number of trees in the forest
283 $\in \{50, 100, 200, 400, 600\}$, maximum tree depth $\in 5\text{--}14$, and a range of 15 values centered around
284 the training set’s length divided by 100 for the minimum number of samples per leaf. The minimum
285 number of samples for splitting a node is set to the minimum number of samples per leaf multiplied
286 by a factor of two. The reference metrics for optimization are the MSE for regression and the ROC
287 AUC for classification. Moreover, the classification models output a probability for each validation
288 sample to belong to the positive class. Then, the probability threshold between zero and one that
289 maximises G-Mean is selected to binarize the output (Brownlee 2021; Swets et al. 2000). No
290 hyper-parameter tuning is needed for the two linear models (MLR and RC).

291 *g. Lead time*

292 We forecast at 1–6 weeks lead time. The models are trained separately for each lead time and
293 do not learn from each other. For instance, the two weeks lead time forecast does not receive the
294 one week lead time forecast as an additional input. Moreover, since our data is averaged via a
295 seven-day rolling mean (see Sec 3b2), weeks are labeled by their central day. A one-week-lead-time
296 prediction leaves no gap between the days used to calculate the one-week lag predictors and the
297 days used to determine the target. For instance, the one-week-lead-time forecast run on June 4th
298 (average over June 1st–June 7th) forecasts June 11th (average over June 8th–June 14th). Similarly,
299 two weeks lead time leave a gap of seven unused days.

300 *h. Reference forecasts*

301 We compare our models’ performance to the (1) climatology, (2) persistence, and (3) ECMWF
302 re-forecasts (hindcasts). (1) For the regression problem, *temperature* anomalies with respect to

303 climatology are forecasted. Thus, the climatology forecast is zero for all times per definition. For
304 the classification problem, we compute the climatology forecast as the mode class for each day of
305 the year. Since, in our dataset, the negative class strongly predominates over the positive class,
306 the climatology forecast is found to be the negative class (no heatwave) for all days of the year.
307 (2) Persistence forecasts predict that the future weather condition will be the same as the present
308 condition. In practice, the persistence forecast is defined as keeping the value from initialization
309 time until verification time. For instance, for the regression forecast at two weeks lead time, the
310 persistence is the *temperature* anomaly two weeks before verification time. (3) The ECMWF
311 sub-seasonal prediction system is initialized twice a week and provides 20-year hindcasts with 11
312 ensemble members integrated over 46 days. The hindcasts used here cover the period 2000–2019
313 and use the model version of the Integrated Forecasting System (IFS) cycle 47r1 (Haiden et al.
314 2019). We use the *temperature* anomalies of the ensemble mean as a reference forecast. The
315 *temperature* anomalies are calculated by removing the lead time dependent climatology at each
316 initialization, calculated by the 20-year mean of the 11-member ensemble started on the same
317 day and month for each year of the reference period (2000–2019). For instance, if a hindcast
318 was initialized on the 31st of May, the lead time dependent climatology corresponding to that
319 hindcast is calculated by the mean of the 11-member ensemble initialized on the 31st of May and
320 averaged over the 20-year reference period (2000–2019) separately for each of the 46 days. For
321 each initialization, after the calculation of the *temperature* anomalies, a 7-day rolling mean was
322 applied. In this way, we end up with 40 days per initialization, with each day being the centre of
323 the 7-day rolling mean. For instance, the first day predicted by the initialization on the 31st of May
324 will be June 4th (average over June 1st–June 7th).

325 *i. Uncertainty estimation*

326 We use the standard deviation of a model ensemble to quantify the uncertainty of the forecasts by
327 the ECMWF and the ML models. For ECMWF, the considered ensemble consists of 11 models.
328 For the RFs, the forecasts by the individual trees in the forest are used. Depending on the hyper-
329 parameter optimization, the number of estimators forming the ensemble can vary between ten and
330 600. Finally, for the linear models, an ensemble of 600 members is created by randomly removing
331 five full (but not necessarily sequential) years from the full training set.

332 **4. Results and discussion**

333 *a. Forecasts*

334 1) REGRESSION FORECASTS

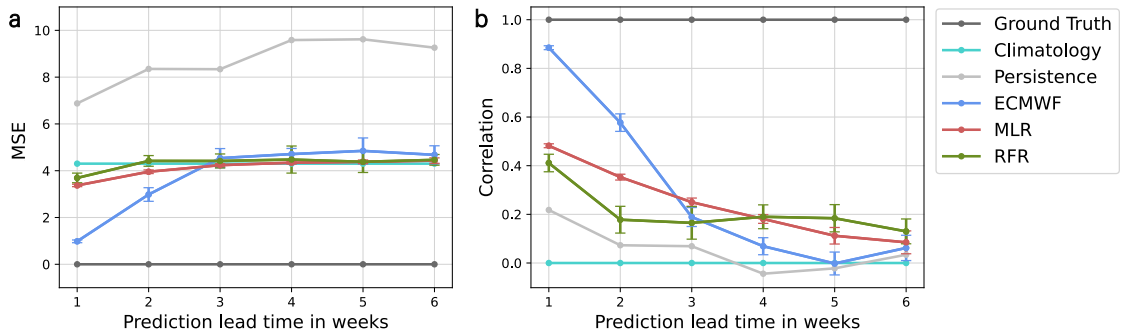


FIG. 4: **Performance of the regression models for six different lead times** (a) MSE and (b) correlation for the regression forecasts. An accurate forecast is characterized by a low MSE and a high correlation. The error bars show the uncertainty of each forecast estimated via the standard deviation of the ensemble mean.

335 In Figure 4, the regression forecasts from two different ML models (MLR and RFR) at six different
336 lead times (1–6 weeks) are compared among each other and to the climatology, persistence, and
337 ECMWF forecasts. The analogous results for nested CV are shown in Figure A2 in the Appendix.
338 As can be observed in Figure 4, all metrics are best for a lead time of one week. The uncertainty
339 in the forecasts by all models, which is represented by the error bars, increases with lead time. For
340 the linear ML model, the performance decays linearly with increasing lead time, with a correlation
341 that ranges from 0.48 for one week lead time to 0.09 for six weeks lead time. For the RF, the
342 correlation decreases overall from one to six weeks lead time (from 0.41 to 0.13), but remains
343 noticeably constant for lead times longer than one week. The evolution of the MSE is similar,
344 but with the difference that it saturates when reaching the MSE value that corresponds to the
345 climatology forecast. The MSE for the best model at each lead time ranges between 3.37 for one
346 week lead time and 4.43 at six weeks lead time.

347 The linear ML model outperforms the RF at short lead times (up to three weeks), but the RF
348 model provides a better forecast at long lead times (5–6 weeks). Both ML models outperform the
349 persistence forecast at all lead times. However, the climatology forecast has a relatively low MSE,
350 since zero variability is a good guess at long lead times, when forecasting becomes difficult. For

351 lead times longer than two weeks, the MSEs of the ML models saturate at the climatology’s MSE
352 and ECMWF has a worse MSE than the climatology forecast. Still, the climatology forecast does
353 not correlate with the ground truth and the ML and ECMWF models outperform climatology at
354 all lead times in terms of correlation, since the models always correlate positively with the ground
355 truth. While ECMWF provides highly skilled forecasts in terms of correlation and MSE for one
356 and two weeks lead time, the skill decreases fast with increasing lead time; for lead times of
357 three weeks and longer, the ML models forecast the temperature anomalies more accurately than
358 ECMWF.

359 The ML models generally pick up the sign of the anomalies but their variability is lower than the
360 one from ECMWF and extreme values are not well-captured (see Fig C1 in the Appendix). For
361 longer lead times, all models lose variability, tending to the climatology forecast. In the case of the
362 ML models, this tendency towards climatology can be a consequence of the loss function. The loss
363 functions for the MLR and the RFR models are the residual sum of squares and the mean-square
364 error, respectively. For the hyper-parameter optimization, the MSE is used. All three metrics
365 measure the distance between the forecast and the target curves. Since forecasting anomalies
366 accurately becomes more difficult with increasing lead time, a model that is trained to minimise the
367 error will tend to forecast the mean of the distribution of possible outcomes, becoming smoother
368 and losing variability compared to the observations (Rasp and Thuerey 2021). ML models trained
369 to optimize alternative loss functions (e.g., the correlation) would be worth exploring.

370 2) CLASSIFICATION FORECASTS

371 The classification models output a probability for each sample in the test set to belong to the
372 positive class (i.e., for a week to be classified as a heatwave week). This probabilities are then
373 binarized via a probability threshold, meaning that a zero (no heatwave) or a one (heatwave) is
374 assigned to each sample in the test set (see Sec 3f). In Figure 5, the probabilistic classification
375 forecasts from two different ML models (RC and RFC) at six different lead times (1–6 weeks)
376 are compared among each other and to the climatology, persistence, and ECMWF forecasts. In
377 Figure 6, the performance of the binary classification forecasts is shown. The analogous results
378 for nested CV are shown in Figures A3 and A4 in the Appendix. Two different indices are used:
379 $+1\sigma$ for warm and $+1.5\sigma$ for extremely warm temperatures (see Sec 3a for the index definitions).

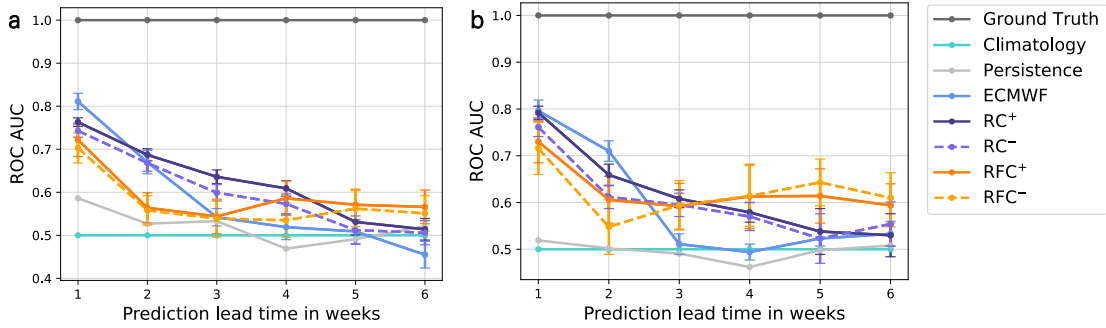


FIG. 5: **Performance of the probabilistic classification models for six different lead times** ROC AUC for the (a) $+1\sigma$ and (b) $+1.5\sigma$ weekly heatwave index. An accurate probabilistic classification forecast is characterized by a high ROC AUC. A no-skill probabilistic classification forecast is represented by a ROC AUC of 0.5, indicated by the climatology. The error bars show the uncertainty of each forecast estimated via the standard deviation of the ensemble mean. Notation: x^+ : oversampled and x^- : undersampled.

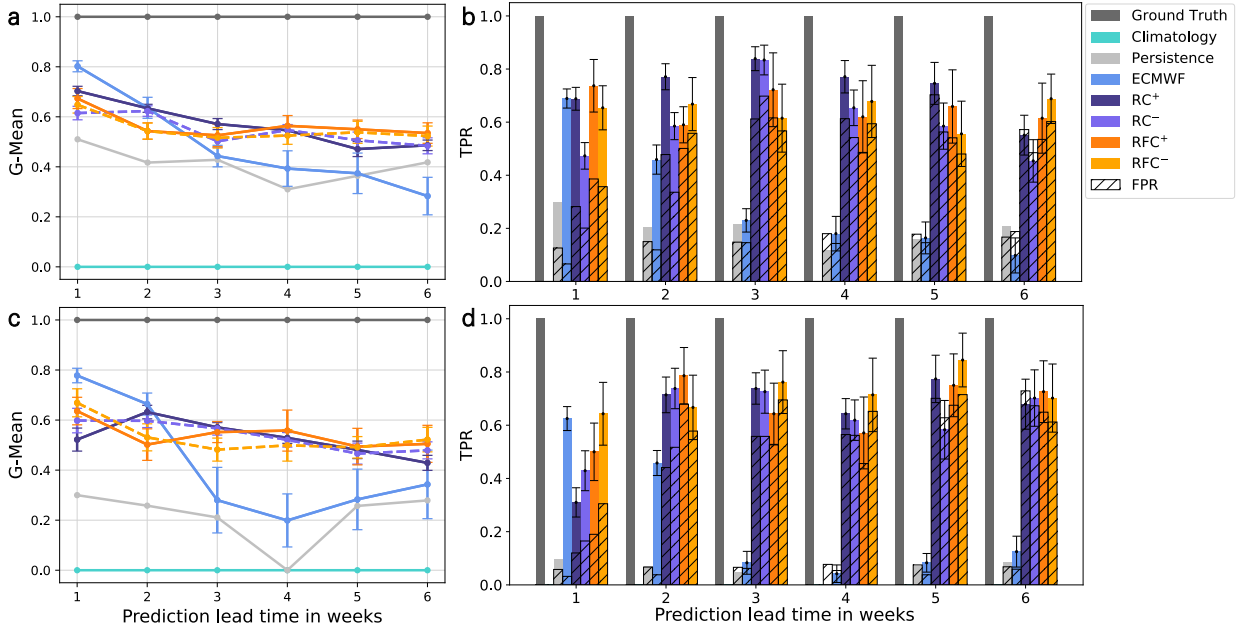


FIG. 6: **Performance of the binary classification models for six different lead times** (a) G-Mean and (b) TPR for the $+1\sigma$ weekly heatwave index. (c) and (d) are the corresponding forecasts for the $+1.5\sigma$ weekly heatwave index. An accurate binary classification forecast is characterized by a high G-Mean. A no-skill binary classification forecast is represented by a G-Mean of zero. The stippled bars in (b) and (d) represent the FPR or False Alarm Rate. The error bars show the uncertainty of each forecast estimated via the standard deviation of the ensemble mean. Since the climatology forecast predicts only zeros (no heatwave), both its TPR and FPR are equal to zero for all lead times. Notation: x^+ : oversampled and x^- : undersampled.

380 The influence of the technique used to balance out the data is also assessed: we compare the
 381 performance of the models when trained on an undersampled (x^-) and on an oversampled (x^+)

382 dataset. Models trained on an unbalanced dataset (with optimized probability threshold) had a
383 slightly lower overall performance (not shown).

384 In general, the linear models have a higher skill than the RFCs for short lead times (up to three
385 weeks). However, two RFCs have a skill that remains more constant than the linear models' skill
386 across lead times and they therefore outperform the linear models for lead times longer than four
387 weeks. Also, the uncertainty in the forecasts by all models increases with lead time. These patterns
388 are analogous to the ones observed for the regression forecast (see Fig 4b). The performance of
389 the best probabilistic forecast decays considerably as the lead time increases (see Fig 5a&b). The
390 ROC AUC for the best model at each lead time is shown in Table 5. Instead, the performance of the
391 best binary classification forecast is more stable, although it also decreases with lead time (see Fig
392 6a&c). Nevertheless, at least one ML model provides a *useful* forecast at each of the considered
393 lead times (1–6 weeks). Meant by *useful* is a ROC AUC above 0.5 for the probabilistic forecast
394 (see Fig 5a&b) and a TPR higher than the FPR for the binary classification (see Fig 6b&d). It is
395 remarkable that non-null skill is present at these long lead times.

396 As for regression, the classification ML models outperform persistence and climatology at all
397 lead times. The persistence forecast has a higher skill when predicting high temperature anomalies
398 ($+1\sigma$) than when predicting extremely high temperature anomalies ($+1.5\sigma$). Our models yield
399 more accurate forecasts than ECMWF for lead times longer than two weeks. At these longer
400 lead times, ECMWF predicts fewer weekly heatwave events than the ML models, having a lower
401 TPR and FPR (see Fig 6b&d). Furthermore, the difference in skill between the ML and ECMWF
402 forecasts at these longer lead times is, in general, more pronounced for the $+1.5\sigma$ index than for
403 $+1\sigma$. The performance of ECMWF in predicting extremely high temperature anomalies ($+1.5\sigma$)
404 drops drastically between two and three weeks lead time. In contrast, ECMWF's classification
405 skill when forecasting high temperature anomalies ($+1\sigma$) decays close to linearly with lead time.
406 Finally, while the oversampled models perform slightly better than the undersampled models for
407 forecasting the $+1\sigma$ weekly heatwave index, there is no clear evidence for one data balancing
408 technique being superior across different indices.

Weekly heatwave index	1 week	2 weeks	3 weeks	4 weeks	5 weeks	6 weeks
$+1\sigma$	0.76 (RC ⁺)	0.69 (RC ⁺)	0.64 (RC ⁺)	0.61 (RC ⁺)	0.57 (RFC ⁺)	0.57 (RFC ⁺)
$+1.5\sigma$	0.79 (RC ⁺)	0.66 (RC ⁺)	0.61 (RC ⁺)	0.61 (RFC ⁻)	0.64 (RFC ⁻)	0.61 (RFC ⁻)

TABLE 5: **ROC AUC scores for the best models** The best model among RC⁺, RC⁻, RFC⁺, and RFC⁻ is chosen for the forecast of each weekly heatwave index at each lead time.

409 *b. Predictor importance*

410 In this section, the relevance of each of the seven predictors for forecasting summer temperature
411 anomalies is discussed. First, a linear correlation analysis is performed. Second, we investigate
412 which lagged predictors were predominantly used by each ML model.

413 1) LINEAR CORRELATION ANALYSIS

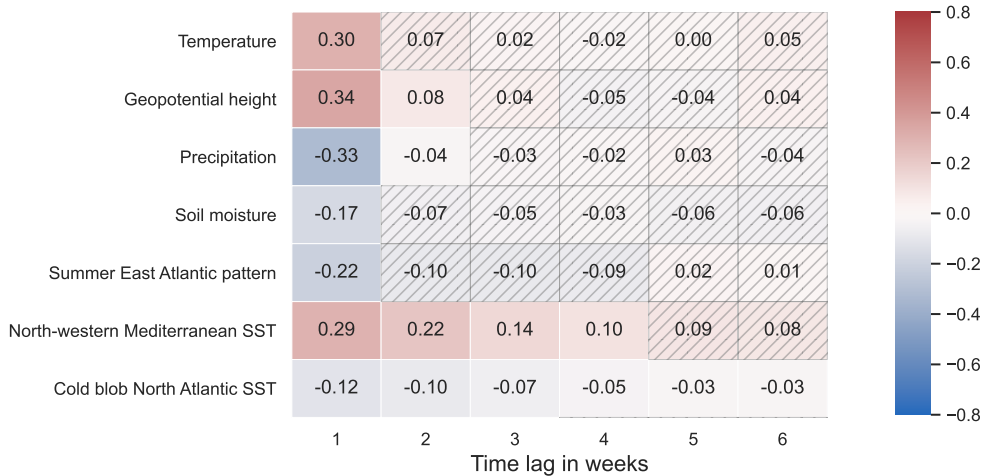


FIG. 7: **Lagged linear correlations between the predictors and the *temperature*** in the extended summer season (MJJAS) at weekly time resolution. When trained with MJJAS data only, our ML models predict summer temperature anomalies and heatwaves with higher accuracy than if the full year is used. Hatched cells correspond to non-significant linear correlations at 5% significance level.

414 In Figure 7, the linear correlations between the *temperature* and the predictors in the extended
415 summer season (MJJAS) are shown for six different time lags (1–6 weeks). At short time lags,
416 the *temperature* shows a strong autocorrelation. The *geopotential* has an even stronger positive
417 correlation to the *temperature*, indicating that during anticyclonic conditions higher temperatures
418 than normal are expected. In contrast, *precipitation*, *soil moisture*, and the *SEA* correlate negatively

419 with *temperature* at short time lags. *Precipitation* is associated with cyclones, cloudy conditions,
420 and lower surface air temperatures (see Sec 2). Moreover, dryness (low *soil moisture*) and high
421 *temperature* reinforce each other (see Sec 2). The correlations with the atmospheric predictors
422 (*temperature*, *geopotential*, *precipitation*, and *SEA*) decay fast. In addition, the linear correlation
423 with *soil moisture* becomes non-significant for lead times of two weeks and longer. In contrast,
424 the SST predictors show a more constant linear correlation over time and dominate on time scales
425 longer than a week, since they are more persistent. While the *NWMED SST* correlates positively
426 with the *temperature* over CE, the *CNAA SST* correlates negatively with both.

427 2) RELEVANCE OF LAGGED PREDICTORS FOR THE MACHINE LEARNING MODELS

428 Each of the seven predictors is provided to the ML models at four time lags, building a set of 28
429 lagged predictors for each lead time (see Sec 3b2). The relevance of a lagged predictor for each
430 ML model is given by the absolute value of its correlation coefficient for the linear models and
431 its feature importance for the RF models. These values are shown in Tables B1 and B2 for the
432 linear models (MLR and RC⁺, respectively) and in Tables B3 and B4 for the RFs (RFR and RFC⁺,
433 respectively) (see Appendix).

434 In general, predictors at short lags are more useful to the models. Also, the longer the forecast's
435 lead time, the higher the contribution from SST becomes. When forecasting the $+1\sigma$ and the
436 $+1.5\sigma$ heatwave indices, the set of relevant lagged predictors is similar. Nevertheless, we can find
437 differences between the two families of models. For instance, the linear models rely more on SSTs
438 than the RFs.

439 (i) *Linear models* For the linear models, SSTs dominate at all lead times. In particular, the
440 *CNAA SST* is the most relevant predictor for the MLR model at all lead times. Nonetheless, the
441 *temperature*, the *precipitation*, and the *soil moisture* at short lags are useful predictors for the MLR
442 model at short lead times (1–2 weeks) as well. In contrast, these lagged predictors are not of use
443 for the RC⁺ model, which relies almost exclusively on SSTs.

444 (ii) *RF models* For the RF models, *temperature*, *geopotential*, *precipitation*, the *SEA* index, and
445 *NWMED SST* at short lags are the most important predictors at short lead times (one week). SSTs
446 are found to dominate for longer lead times (2–6 weeks), without a substantial difference between
447 *CNAA SST* and *NWMED SST*. In addition, *soil moisture* and the *SEA* index are useful at lead times

448 of 3–6 and 1–5 weeks, respectively. At lead times longer than one week, these two predictors have
449 no significant linear correlation with the *temperature* (see Fig 7) and are used by the RF models
450 but not by the linear models. A plausible explanation for this phenomenon is the presence of
451 highly non-linear links between *temperature* and *soil moisture*, and *temperature* and the *SEA* index.
452 The physical mechanism behind the non-linear link between *temperature* and *soil moisture* can be
453 the positive feedback loop described in Section 2. In addition, a non-linear summer atmospheric
454 response to the SEA pattern in Europe was found by Ossó et al. (2020). The SEA pattern might also
455 influence temperature indirectly through surface-atmosphere feedbacks (including soil moisture).
456 These two non-linear links between *temperature* and *soil moisture*, and *temperature* and the *SEA*
457 index would explain the enhanced skill of the RF models compared to the linear models at lead
458 times higher than four weeks (see Sec 4a).

459 **5. Limitations and downstream tasks**

460 In this section, further research ideas to improve the forecast’s accuracy are suggested: (1)
461 promising alternative models, and (2) approaches to overcome the limitations due to a small
462 sample size.

463 (1) The models used in our study belong to the field of classical ML. The complex nature of
464 climate data (e.g., non-linear dependencies between predictors, autocorrelation, and unobserved
465 predictors) poses important challenges to traditional ML models. As discussed in Section 1, DL
466 is also being used for extreme weather forecasting. DL can capture more complex relationships
467 between predictors and target, and might therefore be better suited to describe the mechanisms
468 behind heatwaves, which most likely include non-linear processes. In addition, classical ML
469 approaches benefit from domain specific hand-crafted features to account for dependencies in
470 time or space, but rarely exploit spatio-temporal dependencies exhaustively. In contrast, DL can
471 automatically extract abstract spatio-temporal features (Reichstein et al. 2019). Yet, DL models
472 require larger datasets than the ones used for this study and were therefore not used.

473 (2) One of the main limitations of this study is the size of the dataset. The initial dataset
474 is considerably larger, but precious information gets lost when taking the average over latitude-
475 longitude boxes. It might be interesting to explore the effect of using several smaller sub-boxes
476 instead of one large box. Additional columns could be added to the dataset, such as a box label

477 or its latitude-longitude coordinates. Also, the currently used boxes are rectangular and their
478 coordinates are chosen based on our physical understanding and the correlation to the target. This
479 could be refined by letting an algorithm select sub-regions of different shapes for each predictor
480 based on the correlation of each grid cell to the target (Vijverberg et al. 2020) or even including the
481 spatial information of the predictors (van Straaten et al. 2022). While lower-dimensional models
482 like MLR and RC might not be able to distinguish between distinct mechanisms acting in different
483 regions, RFs are expected to benefit from additional data.

484 6. Conclusions

485 To conclude, we return to the two research questions about the relevant predictors for summer
486 temperature and the potential improvements of heatwave prediction through ML methods, as stated
487 in the Introduction (see Sec 1):

488 (i) At short lead times (1 week), the following variables are found to be the best predictors
489 of summer temperature anomalies and heatwaves in CE: local 2-m air *temperature*, 500-hPa
490 *geopotential*, *precipitation*, and *NWMED SST*. At longer lead times (2–6 weeks), *NWMED* and
491 *CNAA SST* are the most relevant predictors. Moreover, the *SEA* index and *soil moisture* have a
492 linear link with *temperature* at one week lead time and a possible non-linear link at longer lead
493 times (see Sec 4b).

494 (ii) The performance of the linear and RF models used for forecasting summer temperature
495 anomalies and heatwaves in CE decays with lead time but outperforms persistence and climatology
496 at all lead times. ECMWF yields accurate forecasts for 1–2 weeks lead time but our ML models
497 beat ECMWF at lead times longer than two weeks. While the linear models perform better for
498 shorter lead times (1–3 weeks), the RFs take over at lead times longer than four weeks. The
499 regression forecast of summer temperature is better than a random prediction in forecasting the
500 sign of the anomalies at all considered lead times (1–6 weeks). However, extreme values are poorly
501 captured. For the classification problem, at lead times longer than two weeks, the difference in
502 skill between the ML and ECMWF forecasts is more pronounced for extremely warm temperatures
503 ($+1.5\sigma$) than for warm temperatures ($+1\sigma$). At least one out of the ML models yields a *useful*
504 forecast (meaning ROC AUC > 0.5 and TPR > FPR) for each of the considered lead times (1–6
505 weeks) (see Sec 4a). It is remarkable that non-null skill is present at these long lead times.

506 In summary, we show that ML models can help extend the forecasting lead time of summer
507 temperature anomalies and heatwaves to sub-seasonal scales. ML methods are a promising direc-
508 tion for further research in sub-seasonal forecasting. Nevertheless, making better forecasts is not
509 enough. Forecasts acquire value through their ability to influence the decisions made by their users
510 (Murphy 1993). As discussed in the Introduction (see Sec 1), EWS involve not only forecasting
511 the heatwave event, but also triggering effective and timely response plans that target vulnerable
512 populations and regions. This second step must also be successfully implemented to reduce the
513 impact of such damaging events (Merz et al. 2020; White et al. 2021).

514 *Acknowledgments.* This project has received funding from the European Research Council (ERC)
515 under the European Union’s Horizon 2020 research and innovation programme (project "HEAT-
516 forecast", Grant agreement No. 847456). Support from the Swiss National Science Foundation
517 through projects PP00P2_170523 and PP00P2_198896 to Maria Pyrina and Daniela Domeisen is
518 gratefully acknowledged. Judah Cohen is supported by the US National Science Foundation grants
519 AGS-1657748 and PLR-1901352. We thank Ole Wulff for downloading a part of the data used for
520 this study. Also, we appreciate the recommendations from Michael Murphy and Achim Baldus
521 Benet. Finally, we acknowledge Liam Grunwald for improving the English in the manuscript. The
522 authors declare no conflicts of interests.

523 *Data availability statement.* We acknowledge the E-OBS dataset from the EU-FP6 project
524 UERRA¹ and the Copernicus Climate Change Service, and the data providers in the ECA&D
525 project (Cornes et al. 2018).² The ERA-Interim (Dee et al. 2011), ERA5-Land (Muñoz-Sabater
526 et al. 2021), and ERA20C (Poli et al. 2016) data are provided by ECMWF.³ The HadISST data
527 are provided by the Met Office Hadley Centre (Rayner et al. 2003). The ECMWF S2S data are
528 publicly accessible.⁴

¹<https://www.uerra.eu>

²<https://www.ecad.eu>

³www.ecmwf.int

⁴<https://apps.ecmwf.int/datasets/data/s2s>

Nested Cross-Validation

To assess the robustness of our ML models, a CV scheme is implemented. In CV, the model is trained on different data subsets, which reduces overfitting and results in a better generalisation. Moreover, CV removes the dependency on an arbitrarily-selected test set (i.e., from decadal variability here), making the metrics more robust (Vabalas et al. 2019). Here, a nested CV scheme with five outer and two inner splits is used (see Fig A1). The main benefit of nested CV compared to other CV schemes is that the model is trained and tested on the full dataset while maintaining the independence of the test set. This method is, therefore, well-suited for a limited sample size.

Nested CV is generally not used for time series data, since consecutive time steps are strongly correlated. However, since the correlation between the considered predictors decays after a maximum of a few months and only summer data points are selected for this study, summers belonging to different years can be considered independent from each other. To avoid a strong correlation between the sets at the splitting points, the data is split during the winter months.



FIG. A1: **Nested cross-validation scheme** Figure adopted from Vabalas et al. (2019).

The metrics obtained with nested CV (see Figs A2, A3, and A4) are similar, although smoother, compared to the results without CV (see Figs 4, 5, and 6 in Sec 4). The linear models also show a higher skill than the RF models for lead times up to three weeks and the RFs outperform the linear models at 5–6 weeks lead time. While the skill of the ML models at short lead times (up

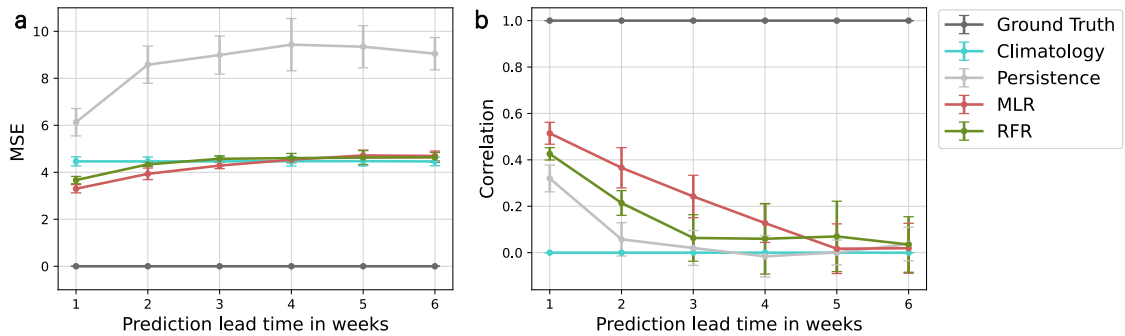


FIG. A2: **Performance of the regression models for six different lead times with nested CV** (a) MSE and (b) correlation for the regression forecasts. An accurate forecast is characterized by a low MSE and a high correlation. The error bars show the uncertainty of each forecast estimated via the standard deviation of the ensemble mean.

547 to three weeks) is similar with and without CV, the models in nested CV perform slightly worse
 548 for longer lead times. Moreover, the uncertainty of the ML models is higher with nested CV
 549 than without. Therefore, while at least two ML models outperform persistence and climatology
 550 in average for all lead times, the error bars overlap with the reference forecasts for lead times of
 551 three weeks and longer. A comparison to the ECMWF forecast can not be included for nested
 552 CV, because the dynamical model is not available during the full test period used for these CV
 553 scheme (1981–2018). Furthermore, the binary classification forecast is found to be considerably
 554 better than the probabilistic classification forecast compared to the reference forecasts. Finally,
 555 the difference between the two data balance methods (under-/ and oversampling) is considerably
 556 dampened by the nested CV and the two approaches can be considered almost equivalent.

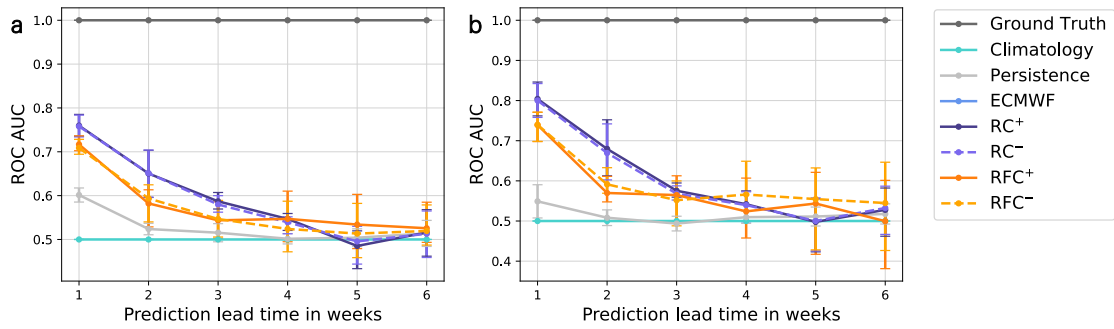


FIG. A3: Performance of the probabilistic classification models for six different lead times with nested CV ROC AUC for the (a) $+1\sigma$ and (b) $+1.5\sigma$ weekly heatwave index. An accurate probabilistic classification forecast is characterized by a high ROC AUC. A no-skill probabilistic classification forecast is represented by a ROC AUC of 0.5, indicated by the climatology. The error bars show the uncertainty of each forecast estimated via the standard deviation of the ensemble mean. Notation: x^+ : oversampled and x^- : undersampled.

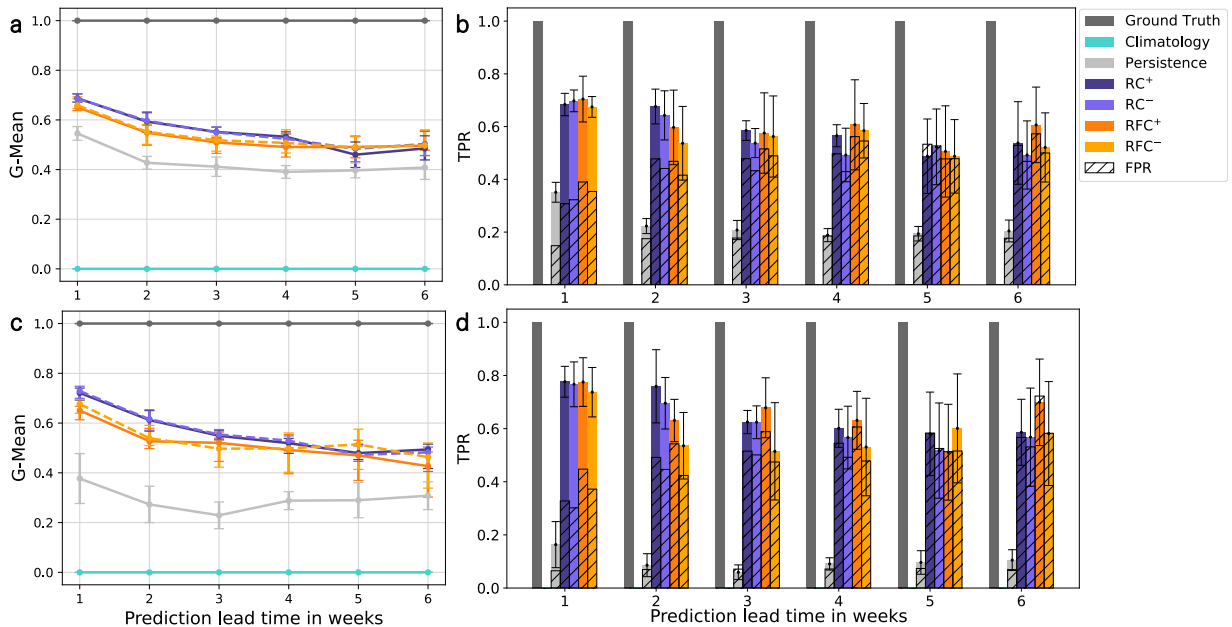


FIG. A4: Performance of the binary classification models for six different lead times with nested CV (a) G-Mean and (b) TPR for the $+1\sigma$ weekly heatwave index. (c) and (d) are the corresponding forecasts for the $+1.5\sigma$ weekly heatwave index. An accurate binary classification forecast is characterized by a high G-Mean. A no-skill binary classification forecast is represented by a G-Mean of zero. The stippled bars in (b) and (d) represent the FPR or False Alarm Rate. The error bars show the uncertainty of each forecast estimated via the standard deviation of the ensemble mean. Since the climatology forecast predicts only zeros (no heatwave), both its TPR and FPR are equal to zero for all lead times. Notation: x^+ : oversampled and x^- : undersampled.

APPENDIX B

Correlation coefficients and feature importances

Lead time		1 week	2 weeks	3 weeks	4 weeks	5 weeks	6 weeks
Predictor	Lag (weeks)						
Temperature	1	0.47	-	-	-	-	-
	2	-0.4	-0.3	-	-	-	-
	3	-0.23	-0.51	-0.42	-	-	-
	4	0.05	0.02	-0.07	-0.12	-	-
	5	-	0.26	0.35	0.31	0.25	-
	6	-	-	0.2	0.33	0.29	0.31
	7	-	-	-	-0.3	-0.22	-0.14
	8	-	-	-	-	-0.15	-0.08
	9	-	-	-	-	-	-0.07
Geopotential	1	0.07	-	-	-	-	-
	2	0.21	0.21	-	-	-	-
	3	0.14	0.33	0.26	-	-	-
	4	-0.21	-0.17	-0.14	-0.12	-	-
	5	-	-0.3	-0.39	-0.36	-0.39	-
	6	-	-	-0.18	-0.35	-0.31	-0.32
	7	-	-	-	0.3	0.15	0.08
	8	-	-	-	-	0.25	0.18
	9	-	-	-	-	-	0.15
Precipitation	1	-0.66	-	-	-	-	-
	2	0.07	0.22	-	-	-	-
	3	0.21	0.27	0.3	-	-	-
	4	-0.03	0.02	0.04	-0.02	-	-
	5	-	-0.05	-0.05	0.03	-0.04	-
	6	-	-	-0.1	-0.01	0.04	-0.05
	7	-	-	-	0.08	0.17	0.13
	8	-	-	-	-	0.2	0.28
	9	-	-	-	-	-	0.33
Soil moisture	1	0.94	-	-	-	-	-
	2	-0.65	-0.08	-	-	-	-
	3	-0.24	-0.28	-0.39	-	-	-
	4	0.03	0.08	-0.04	-0.33	-	-
	5	-	0.03	0.14	-0.01	-0.27	-
	6	-	-	0.08	0	-0.05	-0.17
	7	-	-	-	0.18	-0.06	-0.06
	8	-	-	-	-	0.17	-0.11
	9	-	-	-	-	-	0.03
SEA	1	-0.05	-	-	-	-	-
	2	-0.01	-0.04	-	-	-	-
	3	-0.14	-0.12	-0.12	-	-	-
	4	-0.11	-0.14	-0.14	-0.16	-	-
	5	-	0.17	0.19	0.24	0.19	-
	6	-	-	0.03	0.08	0.13	0.14
	7	-	-	-	0.02	0.04	0
	8	-	-	-	-	0.05	0.04
	9	-	-	-	-	-	-0.1
NWMED SST	1	2.19	-	-	-	-	-
	2	-1.86	3.05	-	-	-	-
	3	-0.06	-3.31	2.07	-	-	-
	4	0.28	0.4	-2.55	1.62	-	-
	5	-	0.46	0.23	-3.24	0.58	-
	6	-	-	0.67	2.23	-1.45	-0.35
	7	-	-	-	-0.27	1.84	0.98
	8	-	-	-	-	-0.71	-0.23
	9	-	-	-	-	-	-0.26
CNAASST	1	-1.93	-	-	-	-	-
	2	2.22	-3.24	-	-	-	-
	3	0.03	3.67	-3.51	-	-	-
	4	-0.3	0.47	3.71	-5.09	-	-
	5	-	-1	1.8	10.26	-1.37	-
	6	-	-	-2.16	-7.29	3.49	1.38
	7	-	-	-	1.95	-4.52	-3.73
	8	-	-	-	-	2.24	3.05
	9	-	-	-	-	-	-0.76

TABLE B1: Regression coefficients for the MLR model Coefficients with absolute values above 0.5 are bold.

Lead time	1 week		2 weeks		3 weeks		4 weeks		5 weeks		6 weeks		
Target	+1 σ	+1.5 σ	+1 σ	+1.5 σ	+1 σ	+1.5 σ	+1 σ	+1.5 σ	+1 σ	+1.5 σ	+1 σ	+1.5 σ	
Predictor	Lag (weeks)												
Temperature	1	0.25	0.31	-	-	-	-	-	-	-	-	-	
	2	-0.23	-0.24	-0.17	-0.15	-	-	-	-	-	-	-	
	3	-0.05	-0.24	-0.23	-0.47	-0.17	-0.34	-	-	-	-	-	
	4	-0.04	-0.07	-0.07	-0.08	-0.13	-0.21	-0.16	-0.25	-	-	-	
	5	-	-	0.1	0.16	0.14	0.23	0.11	0.14	0.1	0.09	-	
	6	-	-	-	-	0.08	0.06	0.12	0.22	0.11	0.22	0.12	0.2
	7	-	-	-	-	-	-	-0.03	-0.3	-0.02	-0.26	-0.02	-0.27
	8	-	-	-	-	-	-	-	-	-0.02	-0.05	0.06	0.05
	9	-	-	-	-	-	-	-	-	-	-	-0.16	-0.31
Geopotential	1	-0.04	-0.15	-	-	-	-	-	-	-	-	-	
	2	0.17	0.27	0.15	0.24	-	-	-	-	-	-	-	
	3	-0.02	0.16	0.14	0.37	0.09	0.28	-	-	-	-	-	
	4	-0.03	-0.07	-0.01	-0.1	0.06	-0.03	0.05	0.01	-	-	-	
	5	-	-	-0.1	-0.08	-0.12	-0.11	-0.09	-0.04	-0.13	-0.05	-	
	6	-	-	-	-	-0.04	-0.09	-0.08	-0.22	-0.07	-0.19	-0.09	-0.16
	7	-	-	-	-	-	-	0.02	0.17	-0.03	0.07	-0.05	0.07
	8	-	-	-	-	-	-	-	-	0.08	0.14	0.05	0.11
	9	-	-	-	-	-	-	-	-	-	-	0.2	0.3
Precipitation	1	-0.3	-0.33	-	-	-	-	-	-	-	-	-	
	2	0.04	-0.01	0.12	0.1	-	-	-	-	-	-	-	
	3	0	0.04	0.06	0.13	0.04	0.13	-	-	-	-	-	
	4	-0.04	0	-0.03	0	-0.01	0.02	-0.01	0.02	-	-	-	
	5	-	-	-0.05	-0.05	-0.04	-0.05	-0.04	-0.01	-0.03	-0.03	-	
	6	-	-	-	-	-0.05	-0.09	-0.03	-0.06	-0.01	-0.01	-0.03	-0.06
	7	-	-	-	-	-	-	0.03	-0.03	0.11	0.02	0.08	0
	8	-	-	-	-	-	-	-	-	0.11	0.07	0.12	0.1
	9	-	-	-	-	-	-	-	-	-	-	0.21	0.24
Soil moisture	1	0.46	0.47	-	-	-	-	-	-	-	-	-	
	2	-0.32	-0.12	-0.07	0.11	-	-	-	-	-	-	-	
	3	0.01	-0.16	-0.01	-0.22	-0.07	-0.14	-	-	-	-	-	
	4	0.02	-0.09	0.09	-0.08	0.03	-0.17	-0.03	-0.26	-	-	-	
	5	-	-	0	0.13	0.05	0.26	0.04	0.13	-0.03	-0.09	-	
	6	-	-	-	-	0.03	-0.04	-0.02	0.11	-0.03	0.05	-0.02	0.04
	7	-	-	-	-	-	-	0.04	-0.06	-0.14	-0.17	-0.12	-0.14
	8	-	-	-	-	-	-	-	-	0.13	0.17	0.1	0.12
	9	-	-	-	-	-	-	-	-	-	-	-0.11	-0.14
SEA	1	-0.1	-0.13	-	-	-	-	-	-	-	-	-	
	2	-0.02	-0.01	-0.04	-0.02	-	-	-	-	-	-	-	
	3	-0.1	-0.14	-0.08	-0.1	-0.09	-0.12	-	-	-	-	-	
	4	-0.1	-0.12	-0.1	-0.12	-0.1	-0.12	-0.1	-0.14	-	-	-	
	5	-	-	0.08	0.15	0.07	0.15	0.08	0.16	0.06	0.12	-	
	6	-	-	-	-	0.05	0.07	0.06	0.1	0.07	0.13	0.08	0.13
	7	-	-	-	-	-	-	0	-0.05	0.01	-0.04	-0.01	-0.07
	8	-	-	-	-	-	-	-	-	0.01	0.06	0.01	0.06
	9	-	-	-	-	-	-	-	-	-	-	-0.03	-0.1
NWMED SST	1	0.98	1.17	-	-	-	-	-	-	-	-	-	
	2	-1.07	-1.3	1.12	1.28	-	-	-	-	-	-	-	
	3	0.4	0.62	-1.06	-1.31	0.71	0.82	-	-	-	-	-	
	4	-0.08	-0.27	0	0.22	-0.68	-0.88	0.58	0.77	-	-	-	
	5	-	-	0.2	0.06	-0.29	0.01	-0.98	-1.14	0.26	0.25	-	
	6	-	-	-	-	0.46	0.27	0.36	0.44	-0.59	-0.1	-0.04	0.45
	7	-	-	-	-	-	-	0.22	0.17	0.47	-0.31	0.13	-0.53
	8	-	-	-	-	-	-	-	-	-0.02	0.37	0	0.09
	9	-	-	-	-	-	-	-	-	-	-	0.01	0.18
CNAASST	1	-0.55	-0.22	-	-	-	-	-	-	-	-	-	
	2	1.29	0.98	-0.73	-0.75	-	-	-	-	-	-	-	
	3	-0.61	-0.82	0.86	0.66	-0.83	-1.22	-	-	-	-	-	
	4	-0.01	0.21	0.13	0.21	0.35	0.79	-1.76	-2.29	-	-	-	
	5	-	-	-0.22	-0.13	1.48	1.2	2.98	3.8	-0.85	-0.98	-	
	6	-	-	-	-	-1.01	-0.83	-1.35	-2.04	1.58	1.1	0.13	-0.39
	7	-	-	-	-	-	-	0.1	0.44	-1	-0.05	-0.4	0.44
	8	-	-	-	-	-	-	-	-	0.23	-0.19	0.55	0.28
	9	-	-	-	-	-	-	-	-	-	-	-0.27	-0.38

TABLE B2: **Regression coefficients for the RC⁺ model** Coefficients with absolute values above 0.5 are bold. The regression coefficients for the RC⁻ model are similar and are not shown here.

Lead time		1 week	2 weeks	3 weeks	4 weeks	5 weeks	6 weeks
Predictor	Lag (weeks)						
Temperature	1	0.02	-	-	-	-	-
	2	0.01	0.02	-	-	-	-
	3	0.01	0.01	0.01	-	-	-
	4	0.01	0.05	0.03	0.01	-	-
	5	-	0.01	0	0.01	0.01	-
	6	-	-	0.01	0.02	0.02	0.02
	7	-	-	-	0.03	0.03	0.01
	8	-	-	-	-	0.01	0.01
	9	-	-	-	-	-	0.01
Geopotential	1	0.23	-	-	-	-	-
	2	0.01	0	-	-	-	-
	3	0.01	0	0.01	-	-	-
	4	0.01	0.01	0.01	0	-	-
	5	-	0	0	0.01	0.01	-
	6	-	-	0	0.01	0.01	0
	7	-	-	-	0.02	0.02	0.01
	8	-	-	-	-	0.01	0
	9	-	-	-	-	-	0.01
Precipitation	1	0.18	-	-	-	-	-
	2	0.03	0.01	-	-	-	-
	3	0.01	0	0.01	-	-	-
	4	0	0	0	0.01	-	-
	5	-	0	0.01	0.01	0.01	-
	6	-	-	0.01	0.02	0.02	0.02
	7	-	-	-	0.01	0	0.01
	8	-	-	-	-	0.01	0
	9	-	-	-	-	-	0.02
Soil moisture	1	0.01	-	-	-	-	-
	2	0.01	0.02	-	-	-	-
	3	0.01	0.01	0.01	-	-	-
	4	0.02	0.01	0.02	0.02	-	-
	5	-	0.04	0.05	0.04	0.05	-
	6	-	-	0.06	0.05	0.05	0.06
	7	-	-	-	0.01	0.01	0.01
	8	-	-	-	-	0.02	0.03
	9	-	-	-	-	-	0.03
SEA	1	0.07	-	-	-	-	-
	2	0.01	0.03	-	-	-	-
	3	0.01	0.01	0.03	-	-	-
	4	0.01	0.01	0.01	0.02	-	-
	5	-	0.06	0.07	0.06	0.05	-
	6	-	-	0.04	0.02	0.02	0.04
	7	-	-	-	0.03	0.03	0.04
	8	-	-	-	-	0.01	0.01
	9	-	-	-	-	-	0.01
NWMED SST	1	0.21	-	-	-	-	-
	2	0.01	0.39	-	-	-	-
	3	0.03	0.04	0.12	-	-	-
	4	0.01	0.03	0.03	0.07	-	-
	5	-	0.01	0.06	0.04	0.05	-
	6	-	-	0.08	0.04	0.05	0.05
	7	-	-	-	0.12	0.1	0.07
	8	-	-	-	-	0.04	0.04
	9	-	-	-	-	-	0.05
CNAASST	1	0.02	-	-	-	-	-
	2	0.02	0.1	-	-	-	-
	3	0.01	0.01	0.13	-	-	-
	4	0.02	0.03	0.03	0.06	-	-
	5	-	0.09	0.06	0.1	0.13	-
	6	-	-	0.12	0.15	0.16	0.22
	7	-	-	-	0.03	0.02	0.01
	8	-	-	-	-	0.07	0.03
	9	-	-	-	-	-	0.16

TABLE B3: Predictor importances for the RFR model Values above 0.04 are bold.

Lead time		1 week		2 weeks		3 weeks		4 weeks		5 weeks		6 weeks	
Target		$+1\sigma$	$+1.5\sigma$	$+1\sigma$	$+1.5\sigma$	$+1\sigma$	$+1.5\sigma$	$+1\sigma$	$+1.5\sigma$	$+1\sigma$	$+1.5\sigma$	$+1\sigma$	$+1.5\sigma$
Predictor	Lag (weeks)												
Temperature	1	0.1	0.1	-	-	-	-	-	-	-	-	-	-
	2	0.01	0.01	0.03	0.02	-	-	-	-	-	-	-	-
	3	0.02	0.03	0.02	0.02	0.02	0.01	-	-	-	-	-	-
	4	0.01	0.03	0.03	0.03	0.02	0.02	0.01	0.02	-	-	-	-
	5	-	-	0.03	0.02	0.02	0.02	0.02	0.02	0.01	0.02	-	-
	6	-	-	-	-	0.02	0.01	0.01	0.02	0.01	0.02	0.01	0.02
	7	-	-	-	-	-	-	0.02	0.04	0.01	0.04	0.01	0.04
	8	-	-	-	-	-	-	-	-	0.02	0.03	0.02	0.03
	9	-	-	-	-	-	-	-	-	-	-	0.02	0.03
Geopotential	1	0.1	0.09	-	-	-	-	-	-	-	-	-	-
	2	0.01	0.01	0.03	0.03	-	-	-	-	-	-	-	-
	3	0.01	0.01	0.02	0.02	0.02	0.02	-	-	-	-	-	-
	4	0.01	0.03	0.02	0.03	0.01	0.02	0.01	0.02	-	-	-	-
	5	-	-	0.03	0.03	0.01	0.01	0.01	0.02	0.01	0.02	-	-
	6	-	-	-	-	0.01	0.01	0.01	0.02	0.01	0.02	0.01	0.02
	7	-	-	-	-	-	-	0.03	0.03	0.02	0.03	0.02	0.03
	8	-	-	-	-	-	-	-	-	0.01	0.02	0.01	0.02
	9	-	-	-	-	-	-	-	-	-	-	0.01	0.02
Precipitation	1	0.13	0.06	-	-	-	-	-	-	-	-	-	-
	2	0.01	0.01	0.03	0.02	-	-	-	-	-	-	-	-
	3	0.01	0.02	0.02	0.02	0.01	0.02	-	-	-	-	-	-
	4	0.01	0.01	0.02	0.02	0.01	0.01	0.01	0.02	-	-	-	-
	5	-	-	0.03	0.02	0.01	0.01	0.01	0.02	0.01	0.02	-	-
	6	-	-	-	-	0.02	0.02	0.02	0.01	0.02	0.02	0.01	0.02
	7	-	-	-	-	-	-	0.01	0.02	0.01	0.02	0.02	0.02
	8	-	-	-	-	-	-	-	-	0.01	0.03	0.02	0.03
	9	-	-	-	-	-	-	-	-	-	-	0.05	0.04
Soil moisture	1	0.03	0.03	-	-	-	-	-	-	-	-	-	-
	2	0.02	0.02	0.03	0.04	-	-	-	-	-	-	-	-
	3	0.01	0.01	0.03	0.03	0.01	0.02	-	-	-	-	-	-
	4	0.01	0.02	0.03	0.03	0.02	0.02	0.02	0.03	-	-	-	-
	5	-	-	0.04	0.04	0.03	0.06	0.03	0.06	0.03	0.05	-	-
	6	-	-	-	-	0.03	0.03	0.04	0.03	0.04	0.03	0.04	0.04
	7	-	-	-	-	-	-	0.03	0.03	0.01	0.03	0.02	0.04
	8	-	-	-	-	-	-	-	-	0.04	0.02	0.05	0.03
	9	-	-	-	-	-	-	-	-	-	-	0.02	0.03
SEA	1	0.09	0.07	-	-	-	-	-	-	-	-	-	-
	2	0.02	0.02	0.04	0.04	-	-	-	-	-	-	-	-
	3	0.03	0.03	0.04	0.05	0.07	0.08	-	-	-	-	-	-
	4	0.02	0.02	0.04	0.03	0.04	0.03	0.05	0.04	-	-	-	-
	5	-	-	0.04	0.05	0.03	0.03	0.03	0.04	0.04	0.04	-	-
	6	-	-	-	-	0.03	0.03	0.03	0.03	0.03	0.03	0.03	0.03
	7	-	-	-	-	-	-	0.02	0.02	0.02	0.02	0.03	0.02
	8	-	-	-	-	-	-	-	-	0.01	0.03	0.02	0.02
	9	-	-	-	-	-	-	-	-	-	-	0.02	0.04
NWMED SST	1	0.09	0.13	-	-	-	-	-	-	-	-	-	-
	2	0.05	0.04	0.08	0.08	-	-	-	-	-	-	-	-
	3	0.03	0.03	0.06	0.06	0.08	0.09	-	-	-	-	-	-
	4	0.02	0.02	0.04	0.04	0.05	0.06	0.05	0.04	-	-	-	-
	5	-	-	0.04	0.04	0.06	0.06	0.06	0.04	0.03	0.05	-	-
	6	-	-	-	-	0.05	0.07	0.07	0.06	0.07	0.05	0.06	0.05
	7	-	-	-	-	-	-	0.04	0.05	0.07	0.05	0.04	0.05
	8	-	-	-	-	-	-	-	-	0.04	0.04	0.06	0.04
	9	-	-	-	-	-	-	-	-	-	-	0.06	0.06
CNAASST	1	0.03	0.03	-	-	-	-	-	-	-	-	-	-
	2	0.04	0.03	0.06	0.05	-	-	-	-	-	-	-	-
	3	0.03	0.02	0.05	0.04	0.06	0.04	-	-	-	-	-	-
	4	0.04	0.02	0.04	0.04	0.07	0.04	0.06	0.04	-	-	-	-
	5	-	-	0.06	0.06	0.09	0.07	0.13	0.07	0.12	0.06	-	-
	6	-	-	-	-	0.1	0.09	0.11	0.06	0.16	0.07	0.12	0.06
	7	-	-	-	-	-	-	0.07	0.08	0.08	0.06	0.09	0.06
	8	-	-	-	-	-	-	-	-	0.07	0.06	0.09	0.05
	9	-	-	-	-	-	-	-	-	-	-	0.05	0.06

TABLE B4: **Predictor importances for the RFC⁺ model** Values above 0.04 are bold. The importances for the RFC⁻ model are similar and are not shown here. However, for the $+1\sigma$ heatwave index, the RFC⁻ model relies more strongly on the *soil moisture* and on the *SEA* at long lead times (3–6 weeks) than the RFC⁺ model does.

Regression forecasts

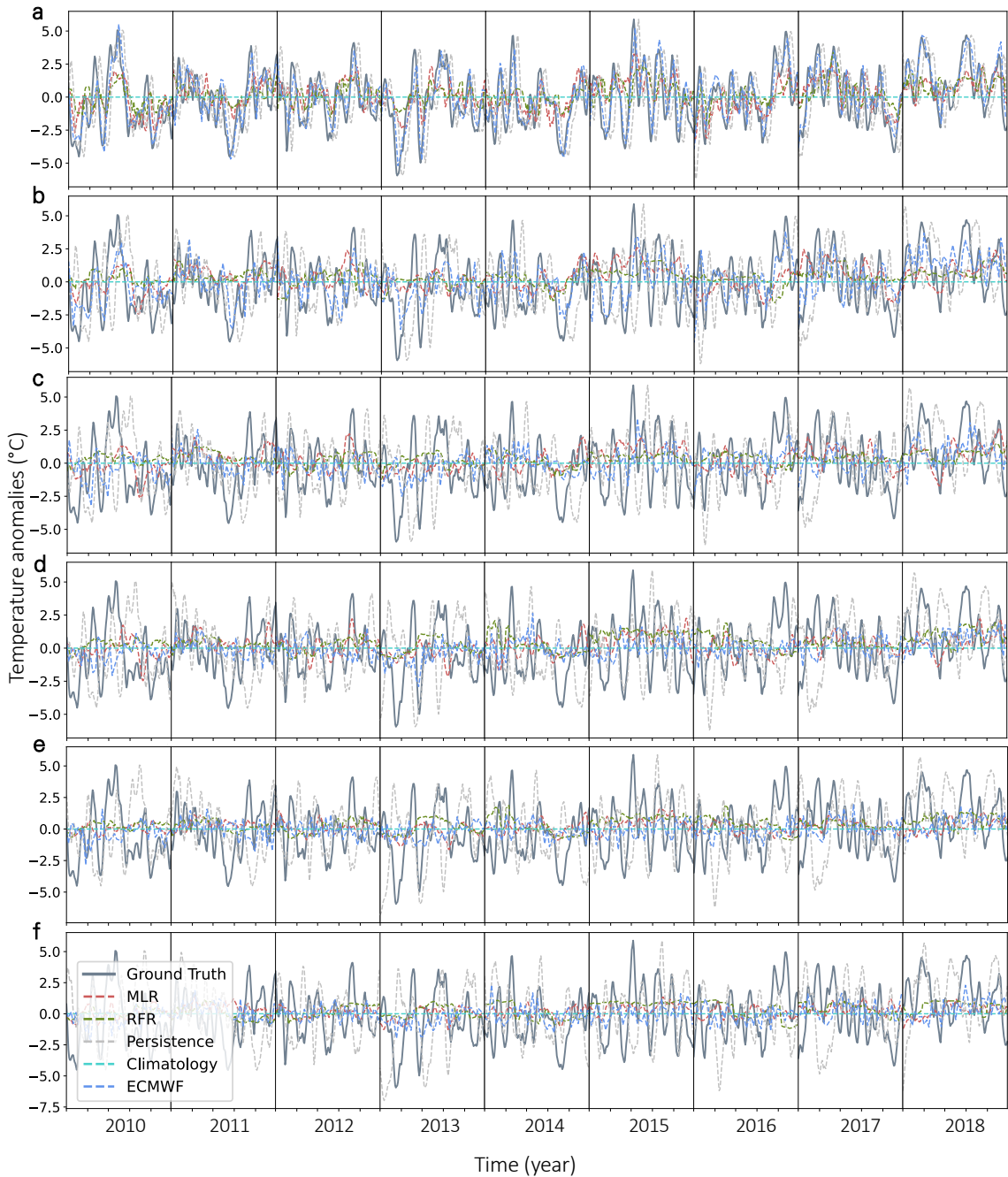


FIG. C1: **Regression time series** The ground truth time series, the reference forecasts, and the predictions by the ML regression models of the temperature anomalies are shown for the nine summers in the test time period (2010–2018). Sub-figures a–f correspond to lead times 1–6, respectively.

561 **References**

- 562 Barriopedro, D., E. M. Fischer, J. Luterbacher, R. M. Trigo, and R. Garcia-Herrera, 2011: The
563 hot summer of 2010: Redrawing the temperature record map of europe. *Science*, **332**, 220–224,
564 <https://doi.org/10.1126/science.1201224>.
- 565 Bassil, K., and D. Cole, 2010: Effectiveness of public health interventions in reducing morbidity
566 and mortality during heat episodes: a structured review. *International Journal of Environmental*
567 *Research and Public Health*, **7**, 991–1001, <https://doi.org/10.3390/ijerph7030991>.
- 568 Basu, R., 2002: Relation between elevated ambient temperature and mortality: a review of the
569 epidemiologic evidence. *Epidemiologic Reviews*, **24**, 190–202, [https://doi.org/10.1093/epirev/](https://doi.org/10.1093/epirev/mxf007)
570 [mxf007](https://doi.org/10.1093/epirev/mxf007).
- 571 Black, E., M. Blackburn, G. Harrison, B. Hoskins, and J. Methven, 2004: Factors contributing to
572 the summer 2003 european heatwave. *Weather*, **59**, 217–223, <https://doi.org/10.1256/wea.74.04>.
- 573 Bladé, I., B. Liebmann, D. Fortuny, and G. J. van Oldenborgh, 2011: Observed and simulated
574 impacts of the summer nao in europe: Implications for projected drying in the mediterranean
575 region. *Climate Dynamics*, **39**, 709–727, <https://doi.org/10.1007/s00382-011-1195-x>.
- 576 Bradley, A. P., 1997: The use of the area under the roc curve in the evaluation of machine learn-
577 ing algorithms. *Pattern Recognition*, **30**, 1145–1159, [https://doi.org/10.1016/s0031-3203\(96](https://doi.org/10.1016/s0031-3203(96)
578 [00142-2](https://doi.org/10.1016/s0031-3203(96).
- 579 Brownlee, J., 2020: A gentle introduction to threshold-moving for imbalanced classification. URL
580 <https://machinelearningmastery.com/threshold-moving-for-imbalanced-classification/>.
- 581 Brownlee, J., 2021: *Imbalanced Classification with Python: Choose Better Metrics, Balance*
582 *Skewed Classes, and Apply Cost-sensitive Learning*. v1.3 ed., Ebook, 246–260 pp., URL [https://](https://machinelearningmastery.com/imbalanced-classification-with-python/)
583 machinelearningmastery.com/imbalanced-classification-with-python/.
- 584 Chattopadhyay, A., E. Nabizadeh, and P. Hassanzadeh, 2020: Analog forecasting of extreme-
585 causing weather patterns using deep learning. *Journal of Advances in Modeling Earth Systems*,
586 **12**, 1942–2466, <https://doi.org/10.1029/2019ms001958>.

- 587 Cho, D., C. Yoo, J. Im, and D. Cha, 2020: Comparative assessment of various machine learning-
588 based bias correction methods for numerical weather prediction model forecasts of extreme air
589 temperatures in urban areas. *Earth and Space Science*, **7**, 2333–5084, [https://doi.org/10.1029/
590 2019ea000740](https://doi.org/10.1029/2019ea000740).
- 591 Cornes, R. C., G. van der Schrier, E. J. M. van den Besselaar, and P. D. Jones, 2018: An ensemble
592 version of the e-obs temperature and precipitation data sets. *Journal of Geophysical Research:
593 Atmospheres*, **123**, 9391–9409, <https://doi.org/10.1029/2017jd028200>.
- 594 de Perez, E. C., and Coauthors, 2018: Global predictability of temperature extremes. *Environmental
595 Research Letters*, **13**, 1748–9318, <https://doi.org/10.1088/1748-9326/aab94a>.
- 596 Deb, P., H. Moradkhani, P. Abbaszadeh, A. S. Kiem, J. Engström, D. Keellings, and A. Sharma,
597 2020: Causes of the widespread 2019–2020 australian bushfire season. *Earth's Future*, **8**, 2328–
598 4277, <https://doi.org/10.1029/2020ef001671>.
- 599 Dee, D. P., and Coauthors, 2011: The era-interim reanalysis: configuration and performance of the
600 data assimilation system. *Quarterly Journal of the Royal Meteorological Society*, **137**, 553–597,
601 <https://doi.org/10.1002/qj.828>.
- 602 Dong, B., R. T. Sutton, T. Woollings, and K. Hodges, 2013: Variability of the north atlantic summer
603 storm track: Mechanisms and impacts on european climate. *Environmental Research Letters*, **8**,
604 <https://doi.org/10.1088/1748-9326/8/3/034037>.
- 605 Duchez, A., and Coauthors, 2016: Drivers of exceptionally cold north atlantic ocean temper-
606 atures and their link to the 2015 european heat wave. *Environmental Research Letters*, **11**,
607 <https://doi.org/10.1088/1748-9326/11/7/074004>.
- 608 Fischer, E. M., S. I. Seneviratne, P. L. Vidale, D. Lüthi, and C. Schär, 2007: Soil mois-
609 ture–atmosphere interactions during the 2003 european summer heat wave. *J. Climate*, **20**,
610 5081–5099, <https://doi.org/10.1175/jcli4288.1>.
- 611 Ford, T. W., P. A. Dirmeyer, and D. O. Benson, 2018: Evaluation of heat wave forecasts seamlessly
612 across subseasonal timescales. *Npj Climate and Atmospheric Science*, **1**, [https://doi.org/10.1038/
613 s41612-018-0027-7](https://doi.org/10.1038/s41612-018-0027-7).

614 Haiden, T., M. Janousek, F. Vitart, Z. B. Bouallegue, L. Ferranti, F. Prates, and D. Richardson,
615 2019: Technical memorandum: Evaluation of ecmwf forecasts, including the 2019 upgrade.
616 10.21957/mlvapkke, URL <https://www.ecmwf.int/node/19277>.

617 Kautz, L.-A., O. Martius, S. Pfahl, J. G. Pinto, A. M. Ramos, P. M. Sousa, and T. Woollings, 2022:
618 Atmospheric blocking and weather extremes over the euro-atlantic sector – a review. *Weather
619 and Climate Dynamics*, **3**, 305–336, <https://doi.org/10.5194/wcd-3-305-2022>.

620 Khan, N., S. Shahid, L. Juneng, K. Ahmed, T. Ismail, and N. Nawaz, 2019: Prediction of heat waves
621 in pakistan using quantile regression forests. *Atmospheric Research*, **221**, 1–11, [https://doi.org/
622 10.1016/j.atmosres.2019.01.024](https://doi.org/10.1016/j.atmosres.2019.01.024).

623 Kolstad, E. W., E. A. Barnes, and S. P. Sobolowski, 2017: Quantifying the role of land-atmosphere
624 feedbacks in mediating near-surface temperature persistence. *Quarterly Journal of the Royal
625 Meteorological Society*, **143**, 1620–1631, <https://doi.org/10.1002/qj.3033>.

626 Kretschmer, M., J. Runge, and D. Coumou, 2017: Early prediction of extreme stratospheric
627 polar vortex states based on causal precursors. *Geophysical Research Letters*, **44**, 8592–8600,
628 <https://doi.org/10.1002/2017gl074696>.

629 Kämäräinen, M., P. Uotila, A. Y. Karpechko, O. Hyvärinen, I. Lehtonen, and J. Räisänen, 2019:
630 Statistical learning methods as a basis for skillful seasonal temperature forecasts in europe. *J.
631 Climate*, **32**, 5363–5379, <https://doi.org/10.1175/jcli-d-18-0765.1>.

632 Lehmann, J., M. Kretschmer, B. Schauburger, and F. Wechsung, 2020: Potential for early forecast
633 of moroccan wheat yields based on climatic drivers. *Geophysical Research Letters*, **47**, 94–8276,
634 <https://doi.org/10.1029/2020gl087516>.

635 Lemaitre, G., F. Nogueira, and C. K. Aridas, 2017: Imbalanced-learn: a python toolbox to tackle
636 the curse of imbalanced datasets in machine learning. *Journal of Machine Learning Research*,
637 **18**, 1–5.

638 Li, M., Y. Yao, I. Simmonds, D. Luo, L. Zhong, and X. Chen, 2020: Collaborative impact of the
639 nao and atmospheric blocking on european heatwaves, with a focus on the hot summer of 2018.
640 *Environmental Research Letters*, **15**, <https://doi.org/10.1088/1748-9326/aba6ad>.

641 Liu, Y., and Coauthors, 2016: Application of deep convolutional neural networks for detecting
642 extreme weather in climate datasets. *arXiv*, <https://doi.org/10.48550/ARXIV.1605.01156>.

643 Loughnan, M., 2014: Heatwaves are silent killers. *Geodate*, **37**, 1–10.

644 Lowe, D., K. L. Ebi, and B. Forsberg, 2011: Heatwave early warning systems and adaptation advice
645 to reduce human health consequences of heatwaves. *International Journal of Environmental
646 Research and Public Health*, **8**, 4623–4648, <https://doi.org/10.3390/ijerph8124623>.

647 Mecking, J. V., S. S. Drijfhout, J. J.-M. Hirschi, and A. T. Blaker, 2019: Ocean and atmosphere
648 influence on the 2015 european heatwave. *Environmental Research Letters*, **14**, <https://doi.org/10.1088/1748-9326/ab4d33>.

649

650 Mehta, P., M. Bukov, C.-H. Wang, A. G. Day, C. Richardson, C. K. Fisher, and D. J. Schwab, 2019:
651 A high-bias, low-variance introduction to machine learning for physicists. *Physics Reports*, **810**,
652 1–124, <https://doi.org/10.1016/j.physrep.2019.03.001>.

653 Merz, B., and Coauthors, 2020: Impact forecasting to support emergency management of natural
654 hazards. *Reviews of Geophysics*, **58**, 8755–1209, <https://doi.org/10.1029/2020rg000704>.

655 Mishra, M., 2018: Regularization: an important con-
656 cept in machine learning. URL [https://towardsdatascience.com/
657 regularization-an-important-concept-in-machine-learning-5891628907ea](https://towardsdatascience.com/regularization-an-important-concept-in-machine-learning-5891628907ea).

658 Murphy, A. H., 1993: What is a good forecast? an essay on the nature of goodness in weather
659 forecasting. *Wea. Forecasting*, **8**, 281–293, [https://doi.org/10.1175/1520-0434\(1993\)008<0281:
660 wiagfa>2.0.co;2](https://doi.org/10.1175/1520-0434(1993)008<0281:wiagfa>2.0.co;2).

661 Muñoz-Sabater, J., and Coauthors, 2021: Era5-land: a state-of-the-art global reanalysis
662 dataset for land applications. *Earth System Science Data*, **13**, 4349–4383, [https://doi.org/
663 10.5194/essd-13-4349-2021](https://doi.org/10.5194/essd-13-4349-2021).

664 Oliveira, J. C., E. Zorita, V. Koul, T. Ludwig, and J. Baehr, 2020: Forecast opportunities for
665 european summer climate ensemble predictions using self-organising maps. *Proceedings of the
666 10th International Conference on Climate Informatics*, 67–71, [https://doi.org/10.1145/3429309.
667 3429319](https://doi.org/10.1145/3429309.3429319).

668 Ossó, A., R. Sutton, L. Shaffrey, and B. Dong, 2020: Development, amplification, and decay of at-
669 lantic/european summer weather patterns linked to spring north atlantic sea surface temperatures.
670 *J. Climate*, **33**, 5939–5951, <https://doi.org/10.1175/JCLI-D-19-0613.1>.

671 Pedregosa, F., and Coauthors, 2011: Scikit-learn: Machine learning in python. *Journal of Machine*
672 *Learning Research*, **12**, 2825–2830.

673 Perkins, S. E., 2015: A review on the scientific understanding of heatwaves -their measurement,
674 driving mechanisms, and changes at the global scale. *Atmospheric Research*, **164–165**, 242–267,
675 <https://doi.org/10.1016/j.atmosres.2015.05.014>.

676 Perkins, S. E., and L. V. Alexander, 2013: On the measurement of heat waves. *J. Climate*, **26**,
677 4500–4517, <https://doi.org/10.1175/jcli-d-12-00383.1>.

678 Perkins-Kirkpatrick, S. E., and S. C. Lewis, 2020: Increasing trends in regional heatwaves. *Nature*
679 *Communications*, **11**, <https://doi.org/10.1038/s41467-020-16970-7>.

680 Poli, P., and Coauthors, 2016: Era-20c: An atmospheric reanalysis of the twentieth century. *J.*
681 *Climate*, **29**, 4083–4097, <https://doi.org/10.1175/jcli-d-15-0556.1>.

682 Pyrina, M., M. Nonnenmacher, S. Wagner, and E. Zorita, 2021: Statistical seasonal prediction of
683 european summer mean temperature using observational, reanalysis and satellite data. *Weather*
684 *and Forecasting*, **36**, <https://doi.org/10.1175/waf-d-20-0235.1>.

685 Racah, E., C. Beckham, T. Maharaj, S. E. Kahou, Prabhat, and C. Pal, 2016: Extremeweather:
686 A large-scale climate dataset for semi-supervised detection, localization, and understanding of
687 extreme weather events. *arXiv*, <https://doi.org/10.48550/ARXIV.1612.02095>.

688 Rasp, S., and N. Thuerey, 2021: Data-driven medium-range weather prediction with a resnet
689 pretrained on climate simulations: A new model for weatherbench. *Journal of Advances in*
690 *Modeling Earth Systems*, **13**, 1942–2466, <https://doi.org/10.1029/2020ms002405>.

691 Rayner, N. A., D. E. Parker, E. B. Horton, C. K. Folland, L. V. Alexander, D. P. Rowell, E. C. Kent,
692 and A. Kaplan, 2003: Global analyses of sea surface temperature, sea ice, and night marine air
693 temperature since the late nineteenth century. *Journal of Geophysical Research*, **108**, 148–227,
694 <https://doi.org/10.1029/2002jd002670>.

- 695 Reichstein, M., G. Camps-Valls, B. Stevens, M. Jung, J. Denzler, and N. Carvalhais, 2019: Deep
696 learning and process understanding for data-driven earth system science. *Nature*, **566**, 195–204,
697 <https://doi.org/10.1038/s41586-019-0912-1>.
- 698 Robertson, A. W., A. Kumar, M. Peña, and F. Vitart, 2015: Improving and promoting sub-
699 seasonal to seasonal prediction. *Bull. Amer. Meteor. Soc.*, **96**, ES49–ES53, [https://doi.org/](https://doi.org/10.1175/bams-d-14-00139.1)
700 [10.1175/bams-d-14-00139.1](https://doi.org/10.1175/bams-d-14-00139.1).
- 701 Rudin, C., 2019: Stop explaining black box machine learning models for high stakes decisions
702 and use interpretable models instead. *Nature Machine Intelligence*, **1**, 206–215, [https://doi.org/](https://doi.org/10.1038/s42256-019-0048-x)
703 [10.1038/s42256-019-0048-x](https://doi.org/10.1038/s42256-019-0048-x).
- 704 Seneviratne, S. I., T. Corti, E. L. Davin, M. Hirschi, E. B. Jaeger, I. Lehner, B. Orlowsky, and A. J.
705 Teuling, 2010: Investigating soil moisture–climate interactions in a changing climate: a review.
706 *Earth-Science Reviews*, **99**, 125–161, <https://doi.org/10.1016/j.earscirev.2010.02.004>.
- 707 Seneviratne, S. I., M. G. Donat, B. Mueller, and L. V. Alexander, 2014: No pause in the increase
708 of hot temperature extremes. *Nature Climate Change*, **4**, 161–163, [https://doi.org/10.1038/](https://doi.org/10.1038/nclimate2145)
709 [nclimate2145](https://doi.org/10.1038/nclimate2145).
- 710 Sobhani, N., D. del Vento, and A. Fanfarillo, 2018: Long-lead forecast of heatwaves in the eastern
711 united states using artificial intelligence. *Proceedings of the Amer. Geophysical Union, Fall*
712 *Meeting 2018*.
- 713 Spensberger, C., and Coauthors, 2020: Dynamics of concurrent and sequential central european
714 and scandinavian heatwaves. *Quarterly Journal of the Royal Meteorological Society*, **146**, 2998–
715 3013, <https://doi.org/10.1002/qj.3822>.
- 716 Storch, H. V., and F. W. Zwiers, 2003: *Statistical analysis in climate research*. Cambridge Univer-
717 sity Press, 293–299 pp.
- 718 Suarez-Gutierrez, L., W. A. Mueller, C. Li, and J. Marotzke, 2020: Dynamical and thermodynami-
719 cal drivers of variability in european summer heat extremes. *Climate Dynamics*, **54**, 4351–4366,
720 <https://doi.org/10.1007/s00382-020-05233-2>.

721 Swets, J. A., R. M. Dawes, and J. Monahan, 2000: Psychological science can improve di-
722 agnostic decisions. *Psychological Science in the Public Interest*, **1**, 1–26, [https://doi.org/](https://doi.org/10.1111/1529-1006.001)
723 10.1111/1529-1006.001.

724 US EPA, O., 2016: Climate change indicators: Heat-related deaths. URL [https://www.epa.gov/](https://www.epa.gov/climate-indicators/climate-change-indicators-heat-related-deaths)
725 climate-indicators/climate-change-indicators-heat-related-deaths.

726 Vabalas, A., E. Gowen, E. Poliakoff, and A. J. Casson, 2019: Machine learning algorithm validation
727 with a limited sample size. *PLOS ONE*, **14**, <https://doi.org/10.1371/journal.pone.0224365>.

728 van Straaten, C., K. Whan, D. Coumou, B. van den Hurk, and M. Schmeits, 2022: Using explainable
729 machine learning forecasts to discover sub-seasonal drivers of high summer temperatures in
730 western and central europe. *Mon. Wea. Rev.*, <https://doi.org/10.1175/mwr-d-21-0201.1>.

731 Vijverberg, S., M. Schmeits, K. van der Wiel, and D. Coumou, 2020: Subseasonal statistical
732 forecasts of eastern u.s. hot temperature events. *Mon. Wea. Rev.*, **148**, 4799–4822, [https://doi.org/](https://doi.org/10.1175/mwr-d-19-0409.1)
733 10.1175/mwr-d-19-0409.1.

734 Wallemacq, P., R. Below, and D. McClean, 2018: Economic losses, poverty and disasters (1998–
735 2017). URL <https://www.undrr.org/publication/economic-losses-poverty-disasters-1998-2017>,
736 1–9 pp.

737 White, C. J., and Coauthors, 2017: Potential applications of subseasonal-to-seasonal (s2s) predic-
738 tions. *Meteorological Applications*, **24**, 315–325, <https://doi.org/10.1002/met.1654>.

739 White, C. J., and Coauthors, 2021: Advances in the application and utility of subseasonal-
740 to-seasonal predictions. *Bull. Amer. Meteor. Soc.*, **aop**, 1–57, [https://doi.org/10.1175/](https://doi.org/10.1175/bams-d-20-0224.1)
741 bams-d-20-0224.1.

742 WMO, 2021: Climate adaptation summit: Invest in early warn-
743 ings and early action. URL [https://public.wmo.int/en/media/press-release/](https://public.wmo.int/en/media/press-release/climate-adaptation-summit-invest-early-warnings-and-early-action)
744 climate-adaptation-summit-invest-early-warnings-and-early-action.

745 Wulff, C. O., R. J. Greatbatch, D. I. V. Domeisen, G. Gollan, and F. Hansen, 2017: Tropical forcing
746 of the summer east atlantic pattern. *Geophysical Research Letters*, **44**, 94–8276, [https://doi.org/](https://doi.org/10.1002/2017gl075493)
747 10.1002/2017gl075493.

748 Yiu, T., 2019: Understanding random forest. Towards Data Science, URL [https://](https://towardsdatascience.com/understanding-random-forest-58381e0602d2)
749 towardsdatascience.com/understanding-random-forest-58381e0602d2.

750 Zschenderlein, P., S. Pfahl, H. Wernli, and A. H. Fink, 2020: A lagrangian analysis of upper-
751 tropospheric anticyclones associated with heat waves in europe. *Weather and Climate Dynamics*,
752 **1**, 191–206, <https://doi.org/10.5194/wcd-1-191-2020>.